

ARTICLE

Received 29 Jun 2015 | Accepted 27 Aug 2015 | Published 8 Oct 2015

DOI: 10.1038/ncomms9479

OPEN

# The alternative splicing factor Nova2 regulates vascular development and lumen formation

Costanza Giampietro<sup>1,2,\*</sup>, Gianluca Deflorian<sup>1,\*</sup>, Stefania Gallo<sup>3,4,\*</sup>, Anna Di Matteo<sup>3,5</sup>, Davide Pradella<sup>3,5</sup>, Serena Bonomi<sup>3</sup>, Elisa Belloni<sup>3</sup>, Daniel Nyqvist<sup>6</sup>, Valeria Quaranta<sup>3</sup>, Stefano Confalonieri<sup>1,7</sup>, Giovanni Bertalot<sup>7</sup>, Fabrizio Orsenigo<sup>1</sup>, Federica Pisati<sup>1</sup>, Elisabetta Ferrero<sup>8</sup>, Giuseppe Biamonti<sup>3</sup>, Evelien Fredrickx<sup>9</sup>, Carla Taveggia<sup>9</sup>, Chris D.R. Wyatt<sup>10,11</sup>, Manuel Irimia<sup>10,11</sup>, Pier Paolo Di Fiore<sup>1,7,12</sup>, Benjamin J. Blencowe<sup>13</sup>, Elisabetta Dejana<sup>1,2,14,\*\*</sup> & Claudia Ghigna<sup>3,\*\*</sup>

Vascular lumen formation is a fundamental step during angiogenesis; yet, the molecular mechanisms underlying this process are poorly understood. Recent studies have shown that neural and vascular systems share common anatomical, functional and molecular similarities. Here we show that the organization of endothelial lumen is controlled at the post-transcriptional level by the alternative splicing (AS) regulator Nova2, which was previously considered to be neural cell-specific. Nova2 is expressed during angiogenesis and its depletion disrupts vascular lumen formation *in vivo*. Similarly, Nova2 depletion in cultured endothelial cells (ECs) impairs the apical distribution and the downstream signalling of the Par polarity complex, resulting in altered EC polarity, a process required for vascular lumen formation. These defects are linked to AS changes of Nova2 target exons affecting the Par complex and its regulators. Collectively, our results reveal that Nova2 functions as an AS regulator in angiogenesis and is a novel member of the ‘angioneurins’ family.

<sup>1</sup>FIRC Institute of Molecular Oncology, Via Adamello 16, Milan 20139, Italy. <sup>2</sup>Department of Biosciences, Milan University, Via Celoria 26, Milan 20133, Italy. <sup>3</sup>Istituto di Genetica Molecolare, Consiglio Nazionale delle Ricerche, via Abbiategrasso 207, Pavia 27100, Italy. <sup>4</sup>IUSS—Istituto Universitario di Studi Superiori, Piazza della Vittoria 15, Pavia 27100, Italy. <sup>5</sup>Dipartimento di Biologia e Biotecnologie, ‘Lazzaro Spallanzani’ - Università degli Studi di Pavia, via Ferrata 9, Pavia 27100, Italy. <sup>6</sup>Division of Vascular Biology, Department of Medical Biochemistry and Biophysics, Karolinska Institutet, Stockholm 171 77, Sweden. <sup>7</sup>Dipartimento di Oncologia Sperimentale, Istituto Europeo di Oncologia, Milan 20141, Italy. <sup>8</sup>Department of Oncology, San Raffaele Scientific Institute, via Olgettina 58, Milan 20132, Italy. <sup>9</sup>Division of Neuroscience and INSPE at San Raffaele Scientific Institute, via Olgettina 58, Milan 20132, Italy. <sup>10</sup>EMBL/CRG Research Unit in Systems Biology, Centre for Genomic Regulation (CRG), Barcelona 08003, Spain. <sup>11</sup>Universitat Pompeu Fabra (UPF), Barcelona 08003, Spain. <sup>12</sup>Dipartimento di Scienze della Salute, University of Milan, Milan 20122, Italy. <sup>13</sup>Donnelly Centre for Cellular and Biomolecular Research, University of Toronto, 160 College Street, Toronto, Ontario, Canada M5S 3E1. <sup>14</sup>Rudbeck Laboratory and Science for Life Laboratory, Department of Immunology, Genetics and Pathology, Uppsala University, Dag Hammarskjöldsv 20, Uppsala 751 85, Sweden. \* These authors contributed equally to this work. \*\* These authors jointly supervised this work. Correspondence and requests for materials should be addressed to E.D. (email: elisabetta.dejana@ifom.eu) or to C.G. (email: arneri@igm.cnr.it).

In adulthood most blood vessels remain quiescent; however, in conditions of active physiological tissue growth, such as during embryogenesis or tissue repair, endothelial cells (ECs) migrate and proliferate to form new vessels. This process, known as angiogenesis, is also critical for the pathogenesis of several disorders and to support cancer development and progression<sup>1</sup>. Although angiogenesis does not initiate malignancy, it promotes tumour growth by allowing oxygen and nutrients to reach proliferating cancer cells. Targeting angiogenesis represents a particularly promising anticancer therapeutic approach, and several strategies have been attempted so far<sup>2</sup>.

Recent studies have highlighted significant anatomic, structural and molecular similarities between the vascular and the nervous systems<sup>3</sup>. Both systems possess specialized structures—tip cells at the forefront of endothelial sprouts and axonal growth cones—that, through filopodial extensions, probe the environment for guidance cues. Molecules regulating these processes have been termed ‘angioneurins’<sup>3</sup>. The prototypic angioneurin is the vascular endothelial growth factor (VEGF), which was originally discovered as a key angiogenic factor, but subsequently shown to be important also in the development of the nervous system<sup>4</sup>. Since blood vessels and nerves are functionally interdependent, the malfunctioning of this ‘neurovascular link’ can lead to several vascular and neuronal disorders<sup>3</sup>.

Until now, the many molecular pathways regulating vascular development and angiogenesis have been suggested to act primarily through the regulation of transcription. However, recent studies indicate that post-transcriptional and epigenetic programmes cooperate to confer tissue-specific vascular properties.

Alternative splicing (AS) is a molecular process that generates multiple, distinct mature mRNAs from a primary transcript (pre-mRNA), leading to the production of protein isoforms with different structural and functional properties. Since more than 90% of human multiexonic genes undergo AS<sup>5,6</sup>, this process represents a major mechanism underlying the expansion of the proteome from a limited repertoire of genes<sup>7,8</sup>. AS and transcription predominantly regulate different subsets of genes to generate the molecular and cellular complexity of different cell and tissue types<sup>9–11</sup>. AS thus provides a versatile, additional layer of regulation to both establish and maintain fundamental properties of different cell and tissue types. Despite the importance of AS, the functional roles of the vast majority of AS events is not well understood.

While there are several examples of splicing variants with a role in angiogenesis<sup>12–15</sup>, the molecular mechanisms responsible for their production are still unknown. Here we describe a novel role for *Nova2*, previously described as neural cell-specific<sup>16</sup>, as a key AS regulator of angiogenesis. Both its expression and the levels of AS of its target exons are regulated during this process. Through gain- and loss-of-function approaches in ECs, we show that *Nova2* regulates AS of factors belonging to the Par polarity complex and its regulators. Consequently, vascular lumen formation defects are developed in zebrafish on *nova2* morpholino-mediated knockdown or clustered regularly interspaced short palindromic repeat (CRISPR)-induced genetic mutation. Collectively, our results provide evidence that *Nova2* is a new member of the ‘angioneurins’ family, and further highlight an important biological role for post-transcriptional regulation of exon networks that contribute to both vascular and neuronal functions.

## Results

***Nova2* expression and function are regulated in ECs.** To identify splicing regulatory factors (SRFs) involved in endothelial growth and quiescence, we studied ECs under sparse and

confluent conditions. By mining previously published Affymetrix gene expression data<sup>17</sup> comparing mouse ECs grown at different densities, we identified *Nova2* as an SRF that is significantly upregulated in confluent versus sparse ECs (fold change = 2.3; *P* value < 0.05, Dunnett test). This result was surprising since *Nova2* was considered previously to be neural cell-specific<sup>16</sup>.

*Nova2* and its paralogue *Nova1* are among the best-studied mammalian tissue-specific SRFs. Both proteins bind RNA through KH domains that recognize clusters of YCAAY repeats within the pre-mRNA targets<sup>16</sup>. These factors, with indistinguishable biochemical properties but mutually exclusive expression within the central nervous system (CNS)<sup>18</sup>, regulate AS programmes involved in neuronal development and synapse activity<sup>16</sup>.

Validating the microarray results, we confirmed *Nova2* upregulation in confluent versus sparse ECs using reverse transcription–quantitative PCR (RT–qPCR; Fig. 1a). By comparing *VE-cadherin*-null ECs (VEC-null) with the same cells reconstituted with *VE-cadherin* (VEC-positive)<sup>17</sup> we also found that *Nova2* upregulation in confluent versus sparse ECs does not require *VE-cadherin* expression (Supplementary Fig. 1A). On the contrary, we found that *Nova1* is expressed to a negligible level in ECs, while both factors are expressed in E15.5 mouse whole brain that we used as positive control (Fig. 1a), consistent with recently published results<sup>19,20</sup>. Moreover, expression of the Muscleblind family of tissue-specific AS regulators (*Mbnl1*, *Mbnl2* and *Mbnl3*) was not modified by confluence in ECs (Fig. 1a). We further confirmed the upregulation of *Nova2* in confluent ECs at the protein level by immunoblotting (Fig. 1b). Comparable results were obtained by using another EC line (adult ECs from the mouse lung) under sparse and confluent conditions (Supplementary Fig. 1B). Notably, as in the case of mouse cortex (Fig. 1b) and in human neuroblastoma SH-SY5Y cells (Supplementary Fig. 1C), in ECs the anti-*Nova2*-specific antibody recognized two immunoreactive bands at 50–55 and 70–80 kDa, as previously reported<sup>18</sup>. In agreement with available RNA sequencing (RNAseq) data (Supplementary Fig. 1D), we found that *Nova2* is also expressed in primary human umbilical vein endothelial cells (HUVECs) and that its levels decreased when HUVECs were grown as sparse (Fig. 1c). Moreover, *Nova2* expression increased during endothelial differentiation of mouse embryonic stem (ES) cells (Fig. 1d), or in adult ECs as compared with embryo or fetal ECs (Fig. 1e). Importantly, *Nova2* expression correlated with AS changes of its known target *Ank3*: (i) in sparse versus confluent ECs, (ii) during endothelial differentiation of ES cells and (iii) in ECs of different origin (Fig. 1f) and AS of this target parallels that observed in brain of *Nova2*-null mice<sup>21</sup>. Taken together, these data suggest that *Nova2* expression and function may play a role in vascular maturation.

To confirm the vascular expression of *Nova2* in a more physiological context, we analysed the postnatal mouse retina, which develops a stereotypical vascular pattern following a well-defined sequence of events<sup>22</sup>. In the retina, we found that *Nova2*-positive nuclei were reduced but still present in the ECs at the sprouting front as compared with the central part of the retina where the majority of ECs of the mature vessels (arteries and veins) and capillaries were *Nova2*-positive (Fig. 2a,b and Supplementary Fig. 2A). In addition, we found the specific nuclear expression of *Nova2* in ECs present in the vessels of different tissues, such as normal human thyroid, skin, bladder, colon and prostate (Fig. 2c and Supplementary Fig. 2B).

Collectively, these data indicate that *Nova2* is not exclusively expressed in cells of the nervous system, but it is also present in ECs of different types of vessels.

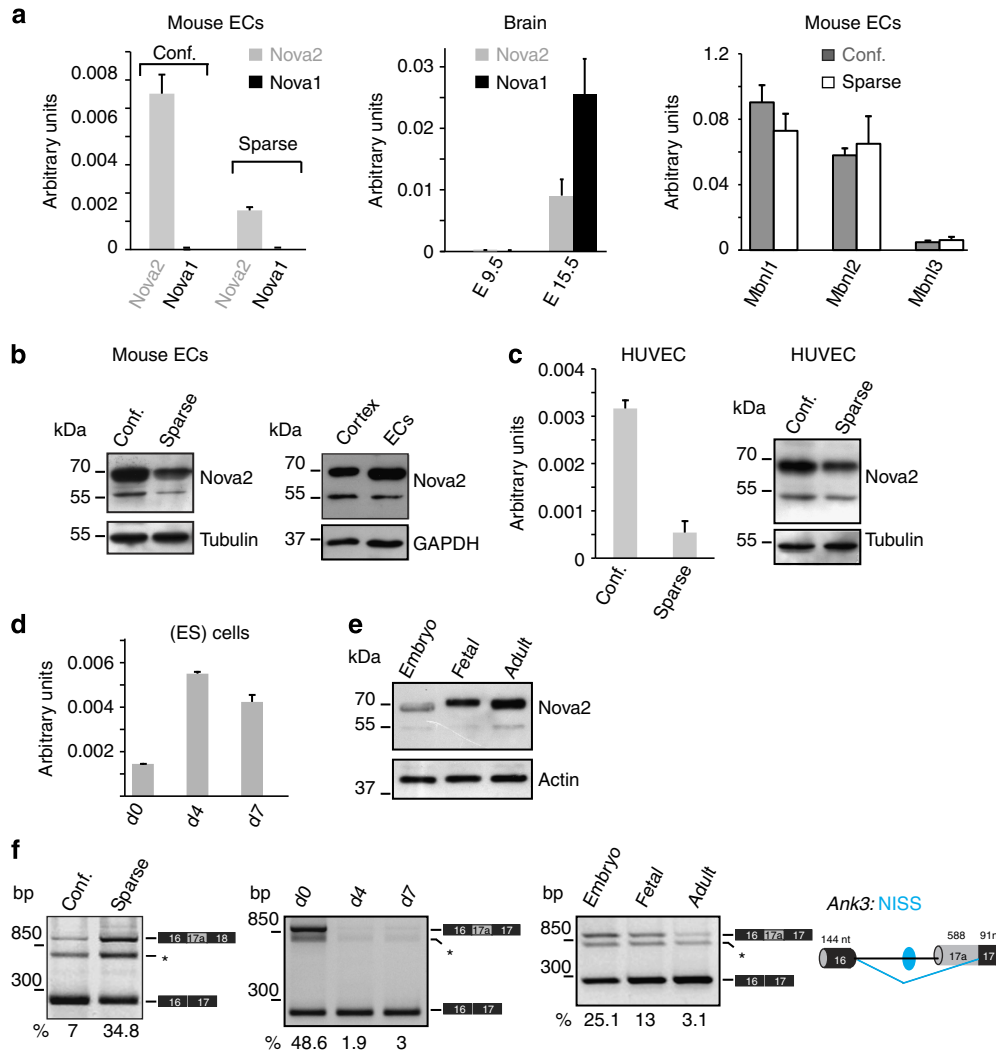


**Figure 1 | Nova2 expression levels and AS of its target are regulated in ECs.** (a) RT-qPCR analysis of *Nova2* and *Nova1* mRNA expression levels in mouse ECs grown as confluent or sparse (left), in E9.5 and E15.5 mouse whole brain (centre), and RT-qPCR analysis of Muscleblind family members (*Mbnl1*, *Mbnl2* and *Mbnl3*) in mouse ECs grown at different densities (right). (b) Immunoblotting analysis of *Nova2* levels in mouse confluent and sparse ECs (left panel; Tubulin as the loading control) and in confluent ECs and the mouse brain cortex (right panel; GAPDH as loading control). (c) *Nova2* mRNA and protein expression levels in HUVECs grown at different densities. (d) RT-qPCR analysis of *Nova2* during endothelial differentiation of mouse ES cells at the indicated times. (e) Immunoblotting analysis of *Nova2* in mouse EC lines derived from whole embryo, fetal heart and adult lung; Actin as the loading control. In all histograms, error bars indicate  $\pm$  s.d. calculated from three independent experiments ( $n = 3$ ). (f) RT-PCR analysis of AS of a known *Nova2* target (*Ankyrin3/Ank3*) in mouse ECs (confluent and sparse; left), during endothelial differentiation of mouse ES cells (centre) and in mouse ECs of different origins (right). The schematic representation of the mouse gene structure (AS exon in grey; constitutive exons in black), the YCAY cluster predicted to function as *Nova2* silencer (blue dot) and the *Nova2*-regulated exon-skipping event (blue bars) are also shown. NISS, *Nova* intronic splicing silencer. The percentage of exon inclusion is shown. Asterisk indicates a nonspecific PCR product.

**Nova2 regulates the endothelial apical-basal polarity.** An important functional similarity in the development of the vascular and nervous systems is the establishment of the apical-basal polarity, as this is a crucial event for the organization of the vascular lumen and for axon guidance<sup>23,24</sup> respectively. Notably, the partitioning-defective (*Par*) polarity complex is a key determinant of cell polarity in both systems<sup>23,24</sup>. The specific localization and activity of the *Par* polarity complex involve the association of four key components: *Par3*, *Par6*, the small GTPase *Cdc42* and the atypical protein kinase C (*PKCζ*). In addition, the small GTPases *Rac1* and *Rap1* are important regulators of the *Par* complex during organization of the vascular lumen<sup>23,25</sup>.

To investigate the role of *Nova2* in the endothelium as a possible regulator of vascular development, we generated stable

*Nova2* knockdown ECs (Fig. 3a). Intriguingly, we found that depletion of *Nova2* expression impairs EC polarity. As shown in Fig. 3b, in two-dimensional (2D) cultures, *Nova2* knockdown altered the subcellular localization of the apical surface marker podocalyxin (*Podxl*) that was distributed all over the cell membrane and also to the basal surface. These findings prompted us to examine whether silencing of *Nova2* alters the junctional staining and/or activity of components of the *Par* polarity complex. *Nova2*-depleted ECs displayed impaired junctional distribution of *Par3*, a multiscaffold protein that promotes the assembly of the *Par* complex (Fig. 3c). Interestingly, *Nova2* knockdown in ECs caused reduced levels of active (GTP-bound) *Cdc42* (Fig. 3d), whose association with the *Par* complex is induced during EC lumen formation<sup>26</sup>. Accordingly, we



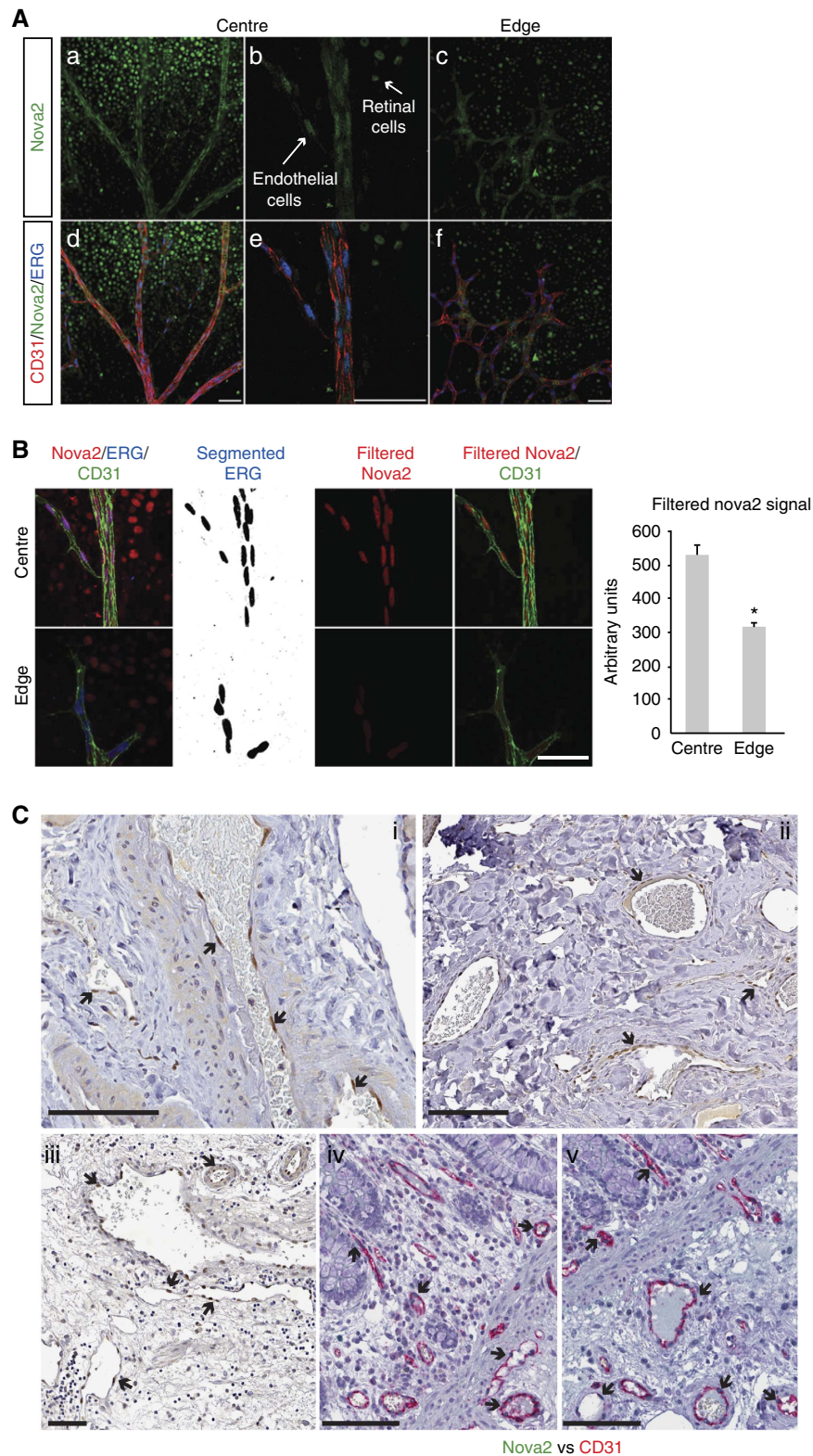


**Figure 2 | Nova2 is expressed in the vascular endothelium *in vivo*.** (a) Immunofluorescence analysis of Nova2 (green), the endothelial markers CD31 (red) and ERG (blue, transcription factor) in whole-mounted postnatal (P6) mouse retina. Optical sections captured using confocal microscopy display large vessels in the central retina region (a,b,d,e) and sprouting ECs in the leading edge of the growing vasculature (c,f). Arrows indicate neural cells of the retina and ECs of vessels expressing Nova2 (scale bar, 50  $\mu$ m). (b) Quantification of Nova2 signal. ERG staining has been segmented with threshold 350–4,096, and segmented images have been filtered to remove speckles and outliers (radius 25). Segmentation results have been used to filter Nova2 staining to isolate EC nuclear staining (scale bar, 50  $\mu$ m). Chart shows average signals (error bars indicate mean  $\pm$  s.d.; asterisks  $P$  value  $< 0.05$ , two-tailed  $t$ -test assuming unequal variances;  $n = 2$ ). (c) IHC of Nova2 in normal human thyroid (i), skin (ii) and bladder (iii) and IHC of Nova2 and the endothelial marker CD31 in normal human colon (iv, v). Arrows indicate Nova2 nuclear staining of ECs in the blood vessels (scale bar, 100  $\mu$ m).

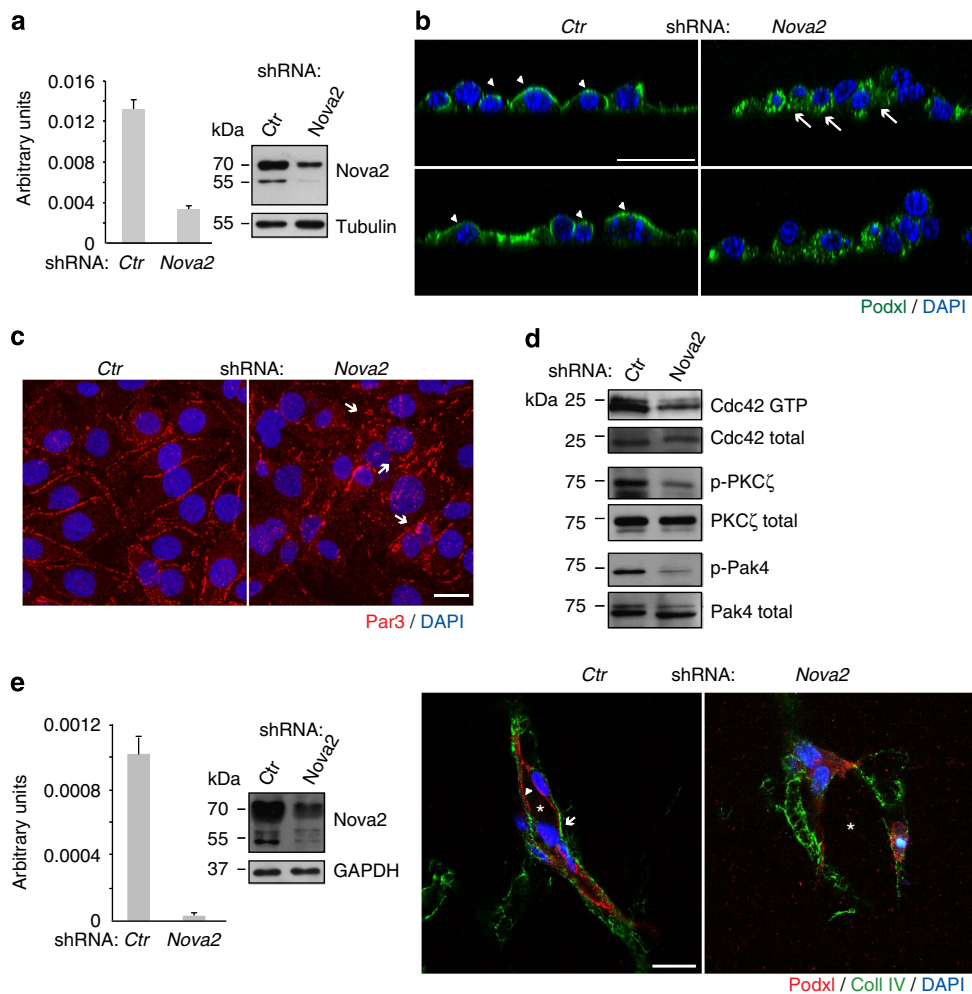


**Figure 3 | Nova2 is required for the EC polarization.** (a) *Nova2* mRNA levels in knockdown mouse ECs (grown as confluent). The *Nova2* protein level was analysed by immunoblotting using an anti-*Nova2* antibody (Tubulin as loading control). (b) Immunofluorescence (IF) analysis of Podocalyxin (Podxl, green) and DAPI (blue) in 2D culture of control (Ctr) and *Nova2*-depleted ECs. Podxl is often distributed to the basal (arrows) instead of the apical surface (arrowheads) in *Nova2*-silenced ECs (confocal sections, z axis; scale bar, 25  $\mu$ m). (c) IF analysis of Par3 (red) and DAPI (blue) in Ctr or *Nova2* knockdown ECs. Arrows indicate altered and fragmented junctional staining of Par3 (bar 20  $\mu$ m). (d) *In vitro* pull down of GTP-bound Cdc42 in Ctr and *Nova2*-silenced ECs. Immunoblotting for the phosphorylation status of PKC $\zeta$  and Pak4 is also shown. (e) Left: *Nova2* mRNA levels in knockdown HUVECs. The *Nova2* protein level was analysed by immunoblotting using an anti-*Nova2* antibody (GAPDH as the loading control). Right: in 3D collagen gel, control HUVECs form vascular structures with a central lumen (asterisk) and apical Podxl and basal collagen IV (Coll IV) proper localization (arrowheads and arrows, respectively), whereas *Nova2*-silenced HUVECs are not correctly polarized (scale bar, 20  $\mu$ m). Error bars indicate mean  $\pm$  s.d. calculated from three independent experiments ( $n = 3$ ).

determined that phosphorylation of PKC $\zeta$ , a Cdc42-GTP-activated protein<sup>27</sup>, is also reduced in *Nova2*-depleted ECs (Fig. 3d). Moreover, *Nova2* knockdown ECs were characterized by reduced levels of phosphorylated Pak4 (p21-activated kinase; Fig. 3d), one of the main Cdc42 downstream effectors<sup>28</sup>.

EC polarization correlates with lumen formation<sup>25,29</sup>. Thus, to test whether *Nova2* is required for the formation of the endothelial lumen, we have carried out its knockdown in primary HUVECs that, when are cultured in three-dimensional (3D) collagen gel, rapidly organize into a network of hollow structures<sup>30</sup>. As shown in Fig. 3e, control HUVEC cells forming vascular-like structures were correctly polarized with Podxl and collagen IV localized to the apical and basal surfaces, respectively. On the contrary, knockdown of *Nova2* resulted in the formation of capillary-like tubular networks with irregular lumen and a non-polarized distribution of endothelial Podxl and collagen IV. These results strongly suggest that *Nova2* splicing factor is crucial for EC morphogenesis.

Recently, the Par polarity complex has been shown to regulate endothelial cell-cell contacts and affect migratory behaviour<sup>25,31</sup>. In agreement with these observations we found that silencing of *Nova2* affected junctional clustering of VEC and  $\beta$ -catenin since the architecture of cell-cell boundaries was partially disorganized in *Nova2* knockdown ECs (Supplementary Fig. 3A). Cell polarity is also established during directional cell migration, where cytoskeletal, adhesive and signalling molecules are distributed asymmetrically. We found that *Nova2* knockdown affected the collective behaviour of migrating ECs. During wound closure, migrating ECs depleted of *Nova2* have in part lost their contacts with neighbouring cells positioned at the back (Supplementary Fig. 3B). The leading edge was more tortuous compared with control ECs (Supplementary Fig. 3B). Finally, given the junctional alterations induced by *Nova2* knockdown, we tested whether endothelial permeability was also modified. We found that the permeability of confluent endothelial monolayers was indeed increased upon *Nova2* depletion (Supplementary Fig. 3C).

To comprehensively identify AS events regulated by *Nova2* in the endothelium, we performed high-throughput RNAseq of two biological replicates of *Nova2* knockdown and control ECs. We used *vast-tools*<sup>32</sup> to identify and quantify all major types of AS events. *vast-tools* maps RNAseq reads to comprehensive sets of annotated and novel splice junctions to derive confident estimates of the percentage of alternative sequence inclusion in a given sample. We identified 365 AS events affected by *Nova2* depletion, including 188 (51.5%) cassette exons (Supplementary Fig. 4, Supplementary Table 1 and see Supplementary Methods for details). Gene Ontology (GO) analyses of AS events predicted to generate alternative protein isoforms (41% of all AS events and 64% of cassette exons; Supplementary Fig. 5) showed a significant enrichment for genes involved in cytoskeleton and cell adhesion (including tight and adherens junctions, and integrin binding), consistent with the phenotypes described above (Supplementary Table 2). In addition, the strongest enriched functional terms corresponded to chromatin remodelling and regulators, suggesting a multilayered impact of *Nova2* regulation on endothelial formation. Finally, we also observed multiple GO terms related to neuronal differentiation and function (for example, neurogenesis, synapsis, axon part and calcium transport), similar to those reported for *Nova*-regulated genes in the brain<sup>16</sup>. Indeed, comparison of differentially included cassette exons in genes expressed in both neurons and ECs (see Supplementary Methods) revealed a highly significant overlap between alternative exons predicted to be regulated by *Nova* proteins in the brain<sup>33</sup> and those showing changes in inclusion levels upon *Nova2* knockdown in the endothelium ( $P=1.93e^{-11}$ , hypergeometric test; Supplementary Fig. 6; Supplementary Table 3), despite the very different approaches used in the two studies (see Supplementary Materials for details).

These newly identified *Nova2* targets expanded the list of previously known targets involved in apical–basal polarity, actin polymerization dynamics and cytoskeletal remodelling, important processes associated with cell polarity, cell shape, motility and adhesion (Supplementary Tables 4 and 5). Thus, to confirm a possible molecular link between these AS events and the phenotypes described above, we analysed AS changes in selected targets using RNA extracted from *Nova2* knockdown ECs (Fig. 4a). Reduced *Nova2* expression in ECs resulted in altered AS of transcripts encoding *Par3*, and regulators of Par activity or localization, including *Magi1*, which recruits Rap1 at junctions<sup>34</sup>, *Rap1GAP* (Rap1 inhibitor)<sup>35</sup>, *Pix- $\alpha$* , *Dock6*, *Dock9* and *DBS* (Cdc42 activators)<sup>36–38</sup> (Fig. 4a and Supplementary Fig. 7). Importantly, these AS changes parallel to those observed in the brain of *Nova2*-null mice<sup>16,33</sup>, or in two stages of brain development (Supplementary Fig. 8A) characterized by different *Nova2* expression levels (Fig. 1a). We confirmed the *Nova2*-dependent AS of target transcripts in RNA samples extracted from *Nova2*-overexpressing ECs (Fig. 4a, Supplementary Fig. 7 and Supplementary Fig. 8B). Notably, the direction of the observed AS changes is consistent with the position of *Nova2*-binding sites (YCAAY; Fig. 4a and Supplementary Fig. 7), as previously reported<sup>16</sup>.

Our data suggest that in cultured ECs *Nova2* establishes EC polarity by controlling *Par3* localization and by regulating the activity of Cdc42. To begin to address the functional relevance of the AS events regulated by *Nova2* in ECs, we focused on the Cdc42 activator *Pix- $\alpha$*  (ref. 36). Our results indicate that *Nova2* promotes the production of a specific *Pix- $\alpha$*  AS isoform lacking exon 17 (*Pix- $\alpha$ - $\Delta$ 17*; Fig. 4a). Intriguingly, we found that *Pix- $\alpha$ - $\Delta$ 17* is more efficient than the *Pix- $\alpha$*  isoform containing exon 17 (*Pix- $\alpha$ -FL*) in rescuing the defect of Cdc42 activity caused by *Nova2* knockdown (Fig. 4b).

Collectively, these results provide evidence that *Nova2* is required for EC polarity and that it acts by inducing AS of a set of key effectors of cell polarity.

***Nova2* promotes vascular lumen formation *in vivo*.** Since EC polarity regulates vascular lumen formation, we tested whether vascular development was affected in the absence of *Nova2*. To this end, we investigated the role of *Nova2* in the embryos and larvae of zebrafish, which constitutes a unique and powerful model to study vertebrate vascular development<sup>39</sup>. Importantly, the *Nova2* RNA-binding domain is 94% identical between zebrafish and human<sup>40</sup>, and we found that a zebrafish *Nova2* orthologous gene (*nova2*) is expressed in the vasculature during development in addition to CNS (Fig. 5a). To assess the role of *nova2* in zebrafish, we performed a morpholino-mediated knockdown of its expression. To specifically visualize the developing blood vessels, we injected morpholino oligos into transgenic embryos expressing the enhanced green fluorescent protein (*EGFP*) gene under the control of the endothelial-specific promoter *fli1a* (*Tg(fli1a:EGFP)y1*)<sup>41</sup>. We used a morpholino targeting the start codon of zebrafish *nova2* (MO-*nova2*) to block translation of both maternal and zygotic *nova2* mRNAs. While embryos injected with a control morpholino displayed a normal morphology, more than 90% of *nova2* morphant embryos showed defects at the level of the forming blood vessels. Moreover, during early embryogenesis the pattern of some intersomitic vessels (ISVs) displayed extra-branching formation and a delay in the connection with the dorsal longitudinal anastomotic vessel (Fig. 5b). Confocal microscopy analysis confirmed that *nova2* knockdown resulted in altered lumen size of both cephalic vessels and of main trunk blood vessels (Fig. 5b,c). To visualize and further characterize the phenotype at the level of the dorsal aorta and posterior cardinal vein, we performed a morphological analysis using transversal paraffin sections stained with haematoxylin–eosin of embryos at different developmental stages (Fig. 5d). The analysis showed that in most of *nova2* morphants the lumen of the dorsal aorta had a larger diameter if compared with controls, through all developmental stages analysed. The lumen of the posterior cardinal vein appeared irregular along the length of the trunk, with areas of enlargement but also few restrictions (Fig. 5d). Furthermore, starting from 2 days of development, even ISVs display an enlarged lumen (Supplementary Fig. 9A). To better characterize the phenotype of *nova2* morphants at the level of ISVs during the angiogenic process, we performed an *in vivo* time lapse imaging assay. As shown in Supplementary Movies 1–3 in *nova2* morphant embryos the apical cells of some ISVs develop many more filopodia and could barely reach the dorsal longitudinal anastomotic vessel. Importantly, co-injection of *nova2* mutants with a morpholino-resistant zebrafish *nova2* mRNA rescued, in more than 60% of the injected embryos, the morphological phenotype of the vessels, confirming the specificity of the effects (Fig. 5b–d and Supplementary Movies 1–3). The abnormal phenotype of blood vessels observed in *nova2* morphants was not due to haemodynamic problems, since at 48 h post fertilization (hpf) the heart appeared normal for size, shape and beat (Supplementary Movies 4 and 5). In addition, EC proliferation and apoptosis were not significantly modified in the morphants (Supplementary Fig. 9B,C). Collectively, these data indicate that *in vivo* *nova2* is required for proper vascular morphogenesis and for the formation of a correct vascular lumen.

Since Par complex members and regulators identified as *Nova2* targets have putative orthologues in zebrafish, we analysed their AS using RNA extracted from *ctr* and *nova2* morphants. Of the investigated pre-mRNAs (Fig. 4a), four (*Rap1GAP*, *Pix- $\alpha$* , *DBS*



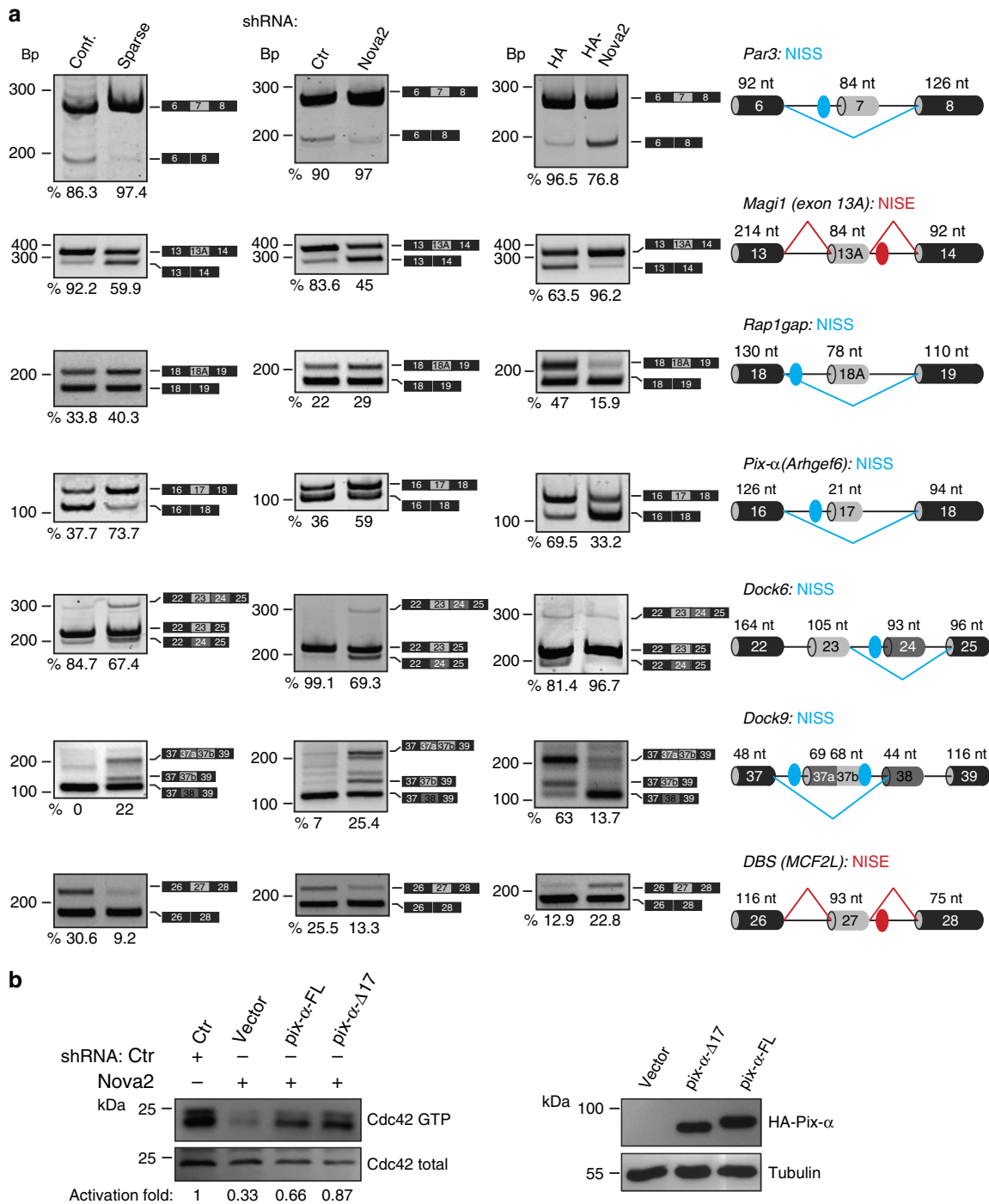


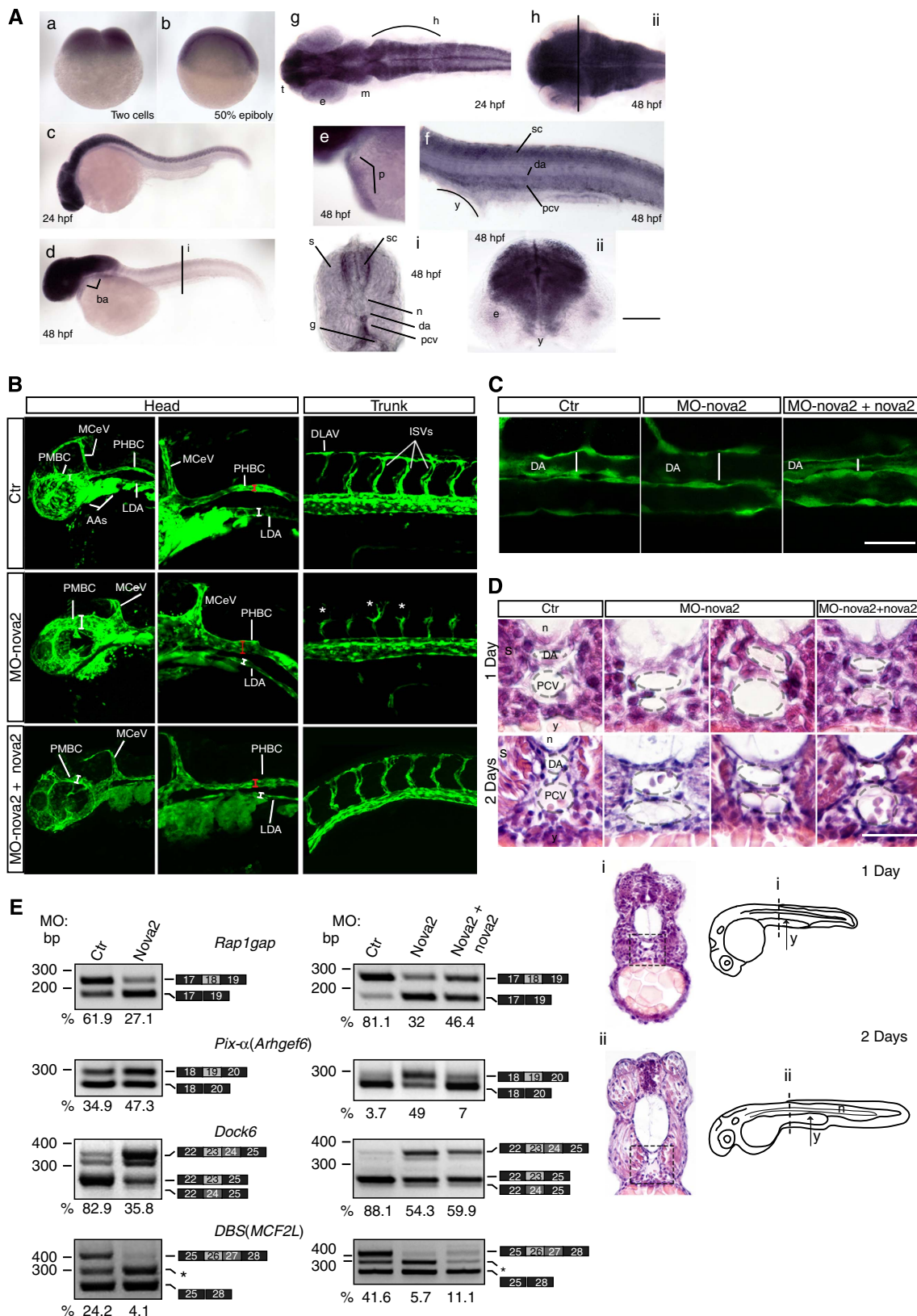
**Figure 4 | AS changes in Nova2 overexpression and knockdown ECs. (a)** AS of the indicated Nova2 targets as determined using RT-PCR in confluent and sparse mouse ECs (left), in confluent Nova2 knockdown ECs (middle) and in sparse ECs overexpressing HA-tagged Nova2 (right). For each gene, the schematic representations of the genomic region containing the AS exon, the transcripts generated from skipping or inclusion of the AS exon and the calculated percentage of exon inclusion are indicated. For *Dock6*, the percentage indicates the ratio between the isoform containing exon 23 (skipping exon 24) and total, whereas for *Dock9* the percentage is the ratio between the isoform containing exon 37a plus 37b and total. Grey boxes, AS exons; black boxes, constitutive exons; blue/red dots indicate YCAY clusters predicted to function as Nova silencer/enhancer. Blue/red bars indicate Nova-silenced/enhanced exon inclusion. NISS, Nova intronic splicing silencer; NISE, Nova intronic splicing enhancer. **(b)** *In vitro* pull down of GTP-bound Cdc42 in Nova2-silenced ECs transfected with the indicated vectors driving the expression of HA-tagged Pix-α deleted of exon 17 (Pix-α-Δ17), Pix-α containing exon 17 (Pix-α-FL) or transfected with the empty vector (vector). The Cdc42 activation fold, calculated as the ratio between GTP-bound Cdc42 and total, is shown (Ctr sample used as a reference value). Pix-α isoform expression was analysed by using anti-HA and Tubulin antibodies.

and *Dock6*) are alternatively spliced in zebrafish (Fig. 5e). Interestingly, in all cases nova2 knockdown alters exon inclusion levels (Fig. 5e) in the direction predicted by the position of

putative Nova-binding motifs<sup>21</sup> (Supplementary Fig. 10). Importantly, aberrant AS events of *nova2* morphants were rescued by co-injection of *nova2* mRNA (Fig. 5e). Of note, we

found that some *nova2* targets (see, for instance, *Rap1gap* and *Pix-α*, Supplementary Fig. 9C) are not expressed at the same level in the different types of vessels suggesting that the effects of the knockdown of *nova2* may have different morphological and functional consequences along the vascular tree.

To assess the apical–basal cell polarity in *nova2* morphant embryos, we analysed the localization of Podocalyxin (Podxl2). As shown in Fig. 6a, in *ctr* embryos Podxl2 is localized at the apical region of the ECs forming ISVs, while in *nova2* morphants Podxl2 is mislocalized in ECs of the ISVs. Moreover, this defect





persisted at late developmental stage (Supplementary Fig. 9A). Likewise, altered *Podxl2* localization was also observed in dorsal aorta of *nova2* morphants (Fig. 6a), suggesting an altered establishment of apical–basal polarity. Again, co-injection of *nova2* mRNA rescued *Podxl2* localization in ECs (Fig. 6a).

Since *Nova2* is expressed in neurons as well as in ECs, and these cells influence their reciprocal differentiation and development<sup>42</sup>, it was important to address whether the vascular phenotype of *nova2* morphants was due to alterations in the nervous or vascular systems. To do this, we used a morpholino-resistant zebrafish *nova2* cDNA, fused with the red fluorescent protein mCherry, under the control of the vasculature-specific *fli1a* promoter (Fig. 6b). The vascular defects in *nova2* morphants were restored by the mosaic transient expression in the vascular endothelium of morpholino-resistant *nova2* cDNA (Fig. 6b–d). Moreover, by generating a zebrafish transgenic line, which stably expresses morpholino-resistant *nova2-mCherry* in the vascular endothelium, we found that injection of MO-*nova2* did not significantly alter blood vasculature morphology (Fig. 6e), indicating that the vascular phenotype of *nova2* morphants is cell autonomous.

To independently validate our findings, we used CRISPRs genome engineering<sup>43</sup> to generate genetic *nova2* mutant fish (Supplementary Fig. 11A and see Methods for details). The characterization of *nova2* mutants strongly supported our results and conclusions obtained using MO-mediated *nova2* knockdown (Supplementary Fig. 11). In particular, *nova2* homozygous mutants displayed overlapping defects with *nova2* morphants, such as shortening of the anteroposterior body axis, reduced head size, curved trunk and slight pericardial oedema (Supplementary Fig. 11B). Moreover, we observed that *nova2* mutants do not develop the swim bladder and display a strong haemorrhagic phenotype visible both at the level of the head and trunk (Supplementary Fig. 11C,D). Notably, similar to *Nova* knockout mice<sup>44,45</sup>, zebrafish *nova2* mutant embryos displayed paralysis. In particular, they have severe difficulty in swimming (probably because of motor–neuronal dysfunction) and died 7–10 days post fertilization, whereas there was no abnormal phenotype in *nova2* heterozygote mutant embryos. Confocal microscopic analyses performed on the *nova2* mutants transgenic for *kdr:EGFP* showed that many blood vessels had an enlarged lumen size, both in the head and in the trunk (Supplementary Fig. 11E), as observed in *nova2* morphant embryos. Similar findings were obtained by histological analysis (Supplementary Fig. 11F). Finally, *nova2* mutants displayed AS changes (Supplementary Fig. 11G) that are comparable to those in *nova2* morphants.

Collectively, our results show that *Nova2* controls the development of the vascular system *in vivo* by modulating endothelial polarity and lumen formation.

## Discussion

Here we report that AS regulation orchestrates some important aspects of EC biology. In particular, our data demonstrate that the AS factor *Nova2*, known to be neural cell-specific<sup>16</sup>, is also expressed in the vascular endothelium and plays a relevant role in vascular morphogenesis.

In spite of its importance, our current understanding of the mechanisms underlying vascular tubulogenesis is only beginning to be unravelled<sup>23,25,29</sup>. We have shown that *Nova2* acts as a post-transcriptional regulator of the molecular mechanisms involved in the organization of the vascular lumen. In zebrafish, depletion and genetic knockout of *nova2* prevents proper formation of the lumen of blood vessels and also results in defects in EC polarization. Interestingly, in avascular organisms, such as *Drosophila melanogaster*, the *Nova* homologue (*Pasilla*, *ps*), is not expressed in the brain, but instead is expressed at high levels in salivary glands and several other non-neuronal tissues<sup>46,47</sup>. Notably, *ps* mutants have altered apical secretion and are characterized by developmental defects of the salivary gland including regions of lumen alteration<sup>46</sup>. This type of morphology, with a severely altered lumen, is somehow reminiscent of the morphology of the zebrafish vasculature observed on *nova2* depletion. Recently, several regulators of salivary gland lumen formation (such as *Cdc42*, *Pak* proteins and *cadherins*) have been identified in *Drosophila*<sup>48</sup>. Intriguingly, they are also implicated in vascular lumenogenesis<sup>23</sup> and, more importantly, regulators of their activity and localization are known *Nova2* AS targets<sup>33</sup>.

Our data show that, in cultured ECs, *Nova2* establishes EC polarity by controlling *Par3* localization, the activity of *Cdc42* and the phosphorylated state of *PKCζ*. Notably, signalling downstream of *Cdc42* is impaired in the absence of *Nova2*, as the active form of *PKCζ* and *Pak4* are reduced in *Nova2*-depleted ECs. Interestingly, *Pak4* phosphorylation correlates with EC lumen formation and RNA interference-mediated suppression of *Pak4* strongly inhibits these processes<sup>26</sup>. Similarly, depletion of *Nova2* impairs the establishment of EC polarity and the organization of the vascular lumen. These defects are associated with aberrant AS of pre-mRNAs encoding factors belonging to the *Par* polarity complex and its regulators.

*Par* complex and downstream effectors play important roles in regulating cell–cell adhesions<sup>25</sup>, in controlling the organization of the microtubule cytoskeleton<sup>49</sup>, and in promoting directional, collective cell migration<sup>31</sup>. Strikingly, we found that downregulation of *Nova2* affected the architecture of cell–cell boundaries and the behaviour of migrating ECs. In particular, in wound closure *Nova2*-depleted ECs failed to move in a cohesive manner with the lack of coordination in the direction of cell movement suggesting that, in addition to its role on lumen

**Figure 5 | *Nova2* is required for vascular lumen formation in zebrafish.** (a) *In situ* hybridization of different zebrafish developmental stages showed *Nova2* expression in the pericardium (p in e), in the trunk vessels (f,i) of 48 hpf embryos and in the CNS of 24 (g) and 48 hpf embryos (h,ii; scale bars, 250 μm in a,b; 125 μm in c,d,g,h); 50 μm in e,f; 25 μm for vibratome sections i,ii). (b) Lateral views of the head and trunk of 28 hpf *Tg(fli1a:EGFP)y1* embryos, expressing the EGFP under the endothelial-specific promoter *fli1a*, injected with control (*ctr*) or morpholino against *nova2* (MO-*nova2*). *Nova2* knockdown results in lumen defects of lateral dorsal aorta (LDA), middle cerebral vein (MCeV) and primordial hindbrain channels (PHBC; compare red and/or white bars length between *ctr* and *nova2* morphants). The ISVs display extra-branching formation (\*) and a delay in the connection with the dorsal longitudinal anastomotic vessel (DLAV). Co-injection of a morpholino-resistant zebrafish *nova2* RNA (MO-*nova2* + *nova2*) rescues the vascular defects. (c) Confocal analysis of the blood vessels in the trunk region of 28-hpf embryos (lateral views); *nova2* morphants display enlarged lumen (white bars) of the dorsal aorta (scale bar, 50 μm). (d) High magnifications of paraffin 10 μm transversal sections, stained with haematoxylin–eosin, of the trunk region of 1- and 2-day embryos (dashed black squares in i,ii) highlighted alterations of the lumen size of the dorsal aorta and PCV in more than 90% of *nova2* morphants. Abnormal phenotype was rescued by co-injection of *nova2* mRNA (scale bar, 50 μm). e, eye; g, gut; h, hindbrain; m, midbrain; n, notochord; s, somite; sc, spinal cord; t, telencephalon; y, yolk; AAs, mandibular arches; PMBC, primordial midbrain channel. (e) *Nova2* knockdown alters the AS of its targets (24 hpf) that is corrected by the co-injection of *nova2* mRNA (28 hpf). The percentage of exon inclusion is indicated (grey, AS exon); *Dock6* as in Fig. 4, *DBS* is the ratio 26 + 27/total. Asterisk, novel *DBS* AS variant containing 75 nt (exon 27b: ACGCAGGTCCTCACATCACTCTCACCCGAGTGAGATGGCTGAGCACTTC TAGTCTGTTGCAGACTAAACGCAGAG) of intron 27.

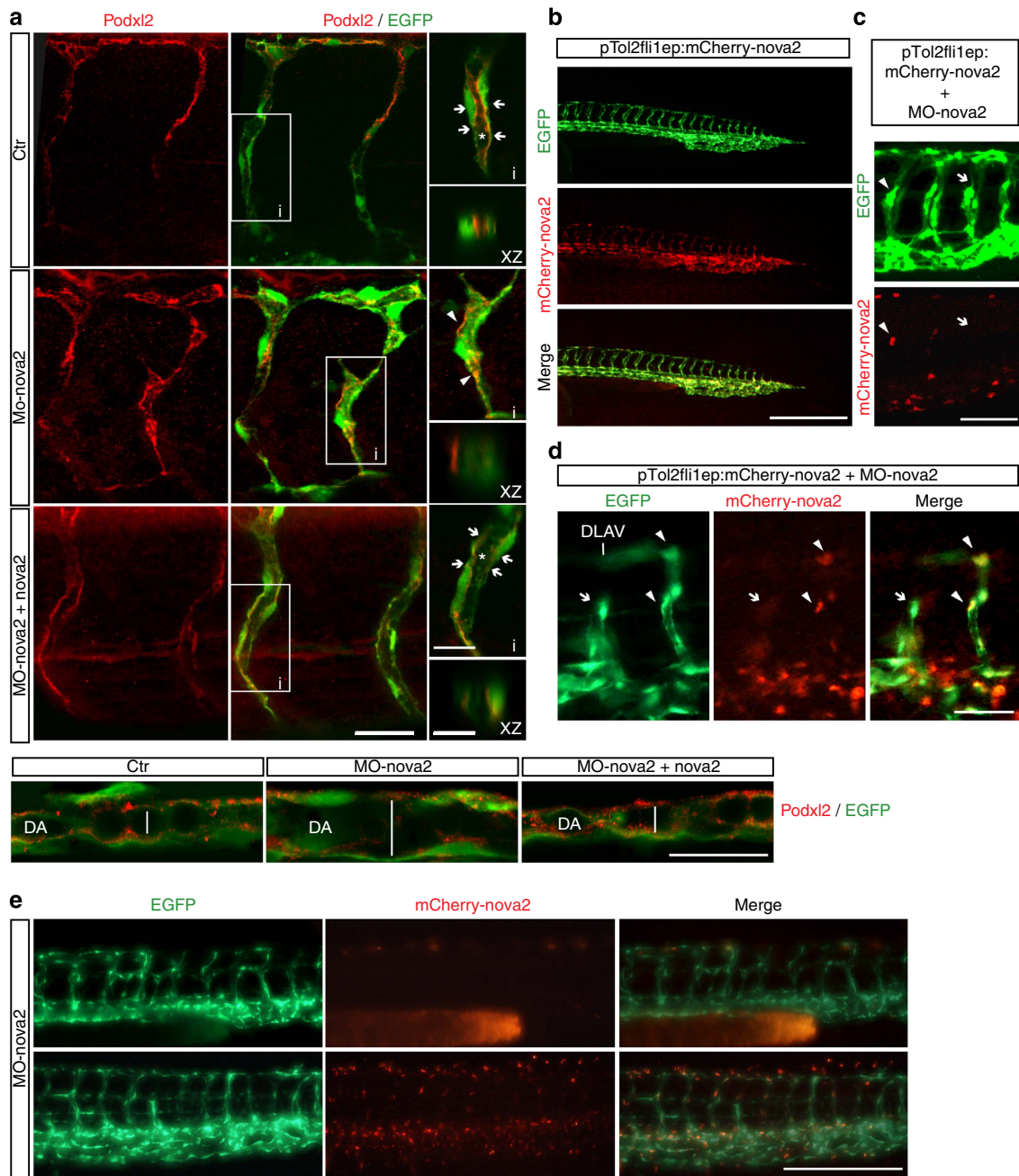


**Figure 6 | Endothelial Nova2 is essential for EC polarization.** (a) *Tg(fli1a:EGFP)y1* zebrafish embryos were treated with control (*ctr*) or *nova2* morpholino (MO-*nova2*) oligos and analysed with anti-Podocalyxin antibody (Podxl2, red) in the ISVs (upper panel). Co-injection of a morpholino-resistant zebrafish *nova2* mRNA was able to rescue the apical-membrane staining (arrow) of Podxl2 in *nova2* morphant (MO-*nova2* + *nova2*; scale bar, 20  $\mu$ m). Areas (i) are magnified on the right (scale bar, 10  $\mu$ m). This is also visualized in the optical transverse sections (XZ, scale bar, 5  $\mu$ m). Asterisk, lumen; arrowheads indicate Podxl2 mislocalization. Lower panel: Podxl2 localization in the dorsal aorta (scale bar, 50  $\mu$ m). (b) Lateral view of the *Tg(fli1a:EGFP)y1* embryo with EGFP under the control of the endothelial-specific promoter *fli1a*. The same transgenic zebrafish embryos were co-injected at one-cell stage with a vector (pTol2fli1ep:mCherry-*nova2*) driving the expression of a morpholino-resistant zebrafish *nova2* mRNA fused to mCherry fluorescent protein under the *fli1a* promoter. In this case individual ECs were mosaically labelled with mCherry-*nova2* expression (*nova2*, red) in the nucleus of some cells of the trunk blood vessels (scale bar, 250  $\mu$ m). (c) Endothelial-autonomous rescue of *nova2* morphants. pTol2fli1ep:mCherry-*nova2* plasmid was co-injected with the *nova2* morpholino oligo (MO-*nova2*) in one-cell stage *Tg(fli1a:EGFP)y1* embryos (bar 40  $\mu$ m; arrowheads and arrows indicate vessels positive and negative for *nova2*, respectively). (d) ISV of the trunk expressing *nova2* (arrowheads) showed a normal pattern and developed a correct lumen, whereas an adjacent ISV (arrows), negative for *nova2* expression, was not formed properly, so that it failed to reach DLAV (scale bar, 30  $\mu$ m). (e) Lateral view of 28-hpf transgenic embryos injected with the MO-*nova2*. Embryo showed in the upper row expresses in the vessel endothelium only GFP, whereas the embryo showed in the lower row expresses also a morpholino-resistant *nova2* cDNA fused with mCherry. The presence of *nova2* in the vessel endothelium is sufficient to preserve vessel morphology of *nova2* morphant embryos (scale bar, 50  $\mu$ m).

formation, Nova2 expression might also control adhesion signals and the directional migration of ECs.

Our current lack of knowledge of the functional implications of most AS events makes it difficult to interpret the global impact of the AS changes we have identified. Moreover, it is plausible that additional AS events are regulated by Nova2 in ECs. Nevertheless, we found that the alteration in *Cdc42* activity in *Nova2* knockdown ECs is preferentially reverted by overexpression of a specific AS isoform of *Pix- $\alpha$*  (*Pix- $\alpha$ - $\Delta$ 17*) regulated by Nova2, indicating that AS of this gene plays an important role in *Cdc42* activation.

We found Nova2-dependent AS regulation of zebrafish orthologous genes encoding polarity regulators. Among these, there are well-characterized activators (*Pix- $\alpha$* , *Dock6* and *DBS*) of *Cdc42*, which—in turn—plays an essential role in controlling lumen formation *in vitro* and *in vivo*<sup>26,48,50–52</sup>.

Remarkably, Nova2-regulated pre-mRNA targets encode proteins that interact with each other<sup>16</sup>, suggesting that Nova2 regulates a network of apical–basal polarity regulators and that AS plays an important role in affecting physical interactions between these factors during the organization of the vascular lumen. Hence, the phenotypic changes that we observed on *Nova2* knockdown are likely the integrated effects of several AS changes that may act in a coordinated and non-redundant manner.

On the basis of the fact that Nova2 affects both neural and vascular cell processes, we suggest that Nova2 is a novel member of the ‘angioneurins’ family<sup>3,4</sup>. Interestingly, Nova2 is the only member of the angioneurin family defined so far that functions as post-transcriptional regulator. Malfunctioning or imbalance in angioneurin signalling contributes to various neurological disorders, indicating that non-neuronal defects contribute to these diseases<sup>3</sup>. In line with this, in Alzheimer’s disease patients’ vascular dysfunction can be observed before the onset of the disease, suggesting that vascular alterations might causally contribute to disease initiation or progression<sup>53</sup>. Notably, significant AS changes associated with decreased Nova activity were reported in Alzheimer’s patients<sup>54</sup>. Since Nova2 is an autoimmune target in a severe neurodegenerative disorder paraneoplastic opsoclonus myoclonus ataxia (POMA)<sup>55</sup>, an obvious question is whether POMA patients, in addition to displaying neurological symptoms, also develop vascular abnormalities.

## Methods

**Cell culture.** ECs were isolated by dissection and dissociation with collagenase type I (Roche, 1.5 mg ml<sup>-1</sup>), DNase (Roche, 25  $\mu$ g ml<sup>-1</sup>) at 37 °C for 1 h and by passing through a 40- $\mu$ m cell strainer. ECs were immortalized by infecting them with a retrovirus expressing the polyoma middle-sized T antigen. VEC-null and VEC-positive were grown as sparse or confluent by placing 500,000 cells in 100- and 35-mm Petri dishes, respectively.

Culture medium of mouse ECs, VEC-null and VEC-positive ECs was DMEM (GIBCO) with 20% fetal bovine serum (FBS; HyClone), glutamine (2 mM, Sigma-Aldrich), penicillin/streptomycin (100 U l<sup>-1</sup>, Sigma-Aldrich), sodium pyruvate (1 mM, Sigma-Aldrich), heparin (100  $\mu$ g ml<sup>-1</sup>, from porcine intestinal mucosa; Sigma-Aldrich) and EC growth supplement (5  $\mu$ g ml<sup>-1</sup>, made from calf brain; complete culture medium). HUVECs were isolated from umbilical vein by treatment with Collagenase (Roche, 0.1%, for 30 min at 37 °C) and were cultured in MCDB 131 with EC supplements.

**Mouse ES cell culture.** To obtain endothelial differentiation of mouse ES cells, cells were mildly trypsinized and suspended in Iscove’s modified Dulbecco medium with 15% FBS, 100 U ml<sup>-1</sup> penicillin, 100  $\mu$ g ml<sup>-1</sup> streptomycin, 450  $\mu$ M monothioglycerol, 10  $\mu$ g ml<sup>-1</sup> insulin, 50 ng ml<sup>-1</sup> human recombinant VEGF-A165 (Peprotech Inc.), 2 U ml<sup>-1</sup> human recombinant erythropoietin (Cilag AG) and 100 ng ml<sup>-1</sup> human basic fibroblast growth factor (bFGF) (Genzyme). Cells were seeded in Petri dishes and cultured for 4 or 7 days at 37 °C with 5% CO<sub>2</sub> and 95% relative humidity.

**Lentivirus production and transduction.** GIPZ Lentiviral Nova2 short-hairpin RNAs (shRNAs) were obtained from Open Biosystems, while pLenti-GIII-CMV-humanNova2-HA from THP Medical Products. HEK293T (American Type Culture Collection, CRL-1573) cells were seeded in DMEM-HIGH supplemented with 10% FBS without antibiotics in 60-mm Petri dishes (one Petri per infection). The day after, cells at 60–70% confluence were transfected (calcium phosphate transfection method) using these quantities of DNA: 5  $\mu$ g of packaging plasmid, 5  $\mu$ g of envelope plasmid and 20  $\mu$ g of Nova2 vectors. After 18 h, the medium was replaced with growth medium DMEM supplemented with 20% FBS and 1% penicillin/streptomycin. Cells were incubated for 24 h and the medium containing the lentiviral particles was harvested, filtered using a 0.45- $\mu$ m filter unit and used to infect the cells.

For viral transduction, mouse EC cells were seeded in 100-mm Petri dishes and were infected at 70% of confluence. Cells were incubated overnight with the viral supernatant supplemented with 0.2 mM proline and polybrene (final concentration 8  $\mu$ g ml<sup>-1</sup>; Sigma). After 48 h puromycin selection (3  $\mu$ g ml<sup>-1</sup>) was started and it was continued until all non-infected control cells died (typically, 5 days).

**2D culture.** Mouse ECs transduced with lentiviral vectors carrying shRNA for Nova2 were seeded in 35-mm Petri dishes coated with Gelatin (Difco) 0.1% and cultured for 72 h. The splitting ratio was such that confluence was reached overnight after seeding. For immunofluorescence, ECs were fixed with 4% paraformaldehyde (PFA) and then permeabilized with 0.5% Triton X-100 for 10 min. Blocking (1 h), primary (overnight) and secondary (1 h) antibodies were diluted in PBS with 2% BSA. The following primary antibodies were used: anti-Par3 (1:100 Millipore), anti-Podocalyxin (1:100 R&D), anti-VE-cadherin (1:100 C-19, sc-6458, goat, Santa Cruz Biotechnology) and anti- $\beta$ -catenin (1:50 BD Transduction Laboratories). Secondary antibodies for immunofluorescence were donkey antibodies to the appropriate species conjugated with Alexa Fluor 488, 555 or 647 (dilution 1:200 or 1:400).

For imaging, charge-coupled device camera on epifluorescence microscope (Leica) or Leica TCS SP2 confocal microscopy were used. ImageJ (NIH) was employed for data analysis. Figures were assembled using Adobe Photoshop and Adobe Illustrator. Only adjustments of brightness and contrast were used in the preparation of the figures. For comparison purposes, different sample images of the same antigen were acquired under constant acquisition settings.

**Immunoblot analysis.** Cells were lysed in Laemmli buffer and proteins were separated using SDS-PAGE and analysed with western blotting. The following primary antibodies were used: anti-Nova2 (1:200 Santa Cruz Biotechnology, C-16), anti-GAPDH (1:5,000 Abcam; 1:50,000 AbFrontier), anti-Tubulin (1:100,000 Sigma-Aldrich), anti-total-Pak4 (1:1,000 Cell Signaling), anti-phospho-Pak4 (1:1,000 Cell Signaling), anti-haemagglutinin (HA; 1:1,000 Covance), anti-total-PKC $\zeta$  (1:1,000 Abcam), anti-phospho-PKC $\zeta$  (1:1,000 Cell Signaling) and anti-Actin (1:500 Santa Cruz Biotechnology). The following secondary antibodies linked to horseradish peroxidase (Jackson ImmunoResearch) were used: anti-Mouse (1:10,000), anti-Goat (1:5,000) and anti-Rabbit (1:10,000). Immunostained bands were detected using the chemiluminescent method (Pierce).

**Retinal immunohistochemistry.** All animal work using mice was conducted in accordance with the Swedish Animal Welfare Board at the Karolinska Institutet, Stockholm, Sweden. Eyes retrieved from pups at P6 were fixed in cold 100% MeOH and stored at –20 °C before dissection. After dissection, retinas were incubated in 5% donkey sera, 1% BSA and 0.5% Triton X-100 in PBS overnight and then incubated with antibodies towards Nova2 (Santa Cruz Biotechnology, C-16), PECAM (BD Bioscience, MEC13.3) and ERG (Abcam, ab92513) overnight. For secondary detection, retinas were incubated with fluorescently conjugated antibodies (Jackson ImmunoResearch) and mounted flat with ProLong Gold (Invitrogen).

**Immunohistochemistry.** All procedures involving human samples were approved by the Istituto Europeo di Oncologia (IEO) Ethical Committee. When possible, a written informed consent for research use of biological samples was obtained from all patients, and the research project was approved by the Institutional IEO Ethical Committee. Immunohistochemistry (IHC) was performed using 3- $\mu$ m sections from formalin-fixed and paraffin-embedded tissue samples. Samples were rehydrated through xylene and graded alcohols. Antigen retrieval was accomplished using 10 mM sodium citrate, 0.05% Tween20, pH 6.0. Samples were then incubated with 3% H<sub>2</sub>O<sub>2</sub> for 5 min, followed by 30 min of blocking in 2% BSA and 0.05% Tween20, and then by the incubation with goat anti-Nova2 (1:100 Santa Cruz Biotechnology, C-16) overnight at 4 °C in 2% BSA and 0.02% Tween20. Immunocomplexes were visualized with LSAB + System-HRP, DAKO (K0690) and acquired with the Aperio ScanScope system. Slides were counterstained with haematoxylin for histological evaluation. Double IHC was performed as follows: antigen retrieval was accomplished using 1 mM EDTA, 0.05% Tween. Samples were then incubated with 3% H<sub>2</sub>O<sub>2</sub> for 5 min, followed by 30 min of blocking in 2% BSA and 0.02% Tween20, and then were incubated with a mix of goat anti-Nova2 (1:200) and mouse anti-CD31 (1:60 DAKO, Clone JC70A) in 2% BSA and 0.02% Tween20 for 2 h at room temperature. Immunocomplexes were visualized with an



anti-goat horseradish peroxidase (HRP) detection system (Goat-on-Rodent HRP-Polymer, Biocare Medical), for 30 min at RT, followed by incubation with a Goat Anti-Mouse AP Polymer detection system (MACH 2 Mouse AP-Polymer Biocare Medical) for 30 min at RT. CD31 was visualized in red using the Vulcan Fast Red Chromogen (Biocare Medical) and Nova2 was visualized in green using the Vina Green Chromogen Kit (Biocare Medical) according to the manufacturer's protocol.

**Migration assay.** To analyse cell migration, the wound-healing technique was used. Briefly, confluent EC monolayers on a tissue culture dish were wounded by manually scratching with a pipette tip after an overnight starving, washed with starting medium and incubated at 37 °C for 8 h in complete media containing Mitomycin C (4 µg ml<sup>-1</sup>). The wound-induced cell migration was followed by staining with fluorescent phalloidin (10 µM, Sigma).

**Paracellular flux.** Mouse ECs were seeded on 0.4-µm pore size Transwell Permeable Supports (Corning) cultured in complete culture medium before assaying permeability. Next, fluorescein isothiocyanate dextran (70 kDa; Sigma) was added to the medium of the transwell apical compartment. At different times of incubation, a 50-µl aliquot of the medium was collected from the basal compartment, and the paracellular tracer flux was measured as the amount of fluorescein isothiocyanate dextran in the medium using a fluorometer.

**3D culture in collagen gels.** HUVECs were transduced with GIPZ lentiviral vectors (Open Biosystems) carrying shRNA for Nova2 or control shRNA. Control and Nova2 knockdown HUVECs were cultured in 3D collagen gel. The final cell density in collagen (3.5 mg ml<sup>-1</sup> final concentration collagen type1 from rat tail, High Concentration, BD Biosciences) was 5 × 10<sup>5</sup> cells ml<sup>-1</sup>. Culture medium was 199 with 1% FCS, Insulin-Transferrin-Selenium supplement (Life Technologies), 50 ng ml<sup>-1</sup> phorbol myristate acetate, 50 µg ml<sup>-1</sup> ascorbic acid, 40 ng ml<sup>-1</sup> VEGF and 40 ng ml<sup>-1</sup> bFGF. For confocal microscopy, 190 µl cell suspension in collagen was used for each microwell (µ-slide 80826, Ibidi, Germany). 3D cultures were fixed with 3% PAF for 35 min, quenched with 75 mM NH<sub>4</sub>Cl and 20 mM glycine in PBS, pH 8, for 10 min and blocked with 0.7% FSG and 0.3% Triton X-100 PBS (blocking buffer) for 30 min. Primary and secondary antibodies were incubated overnight at 4 °C. Primary antibody contained 5% donkey serum. Washes in blocking buffer were performed over the course of a day at room temperature. For immunofluorescence, the following primary antibodies were used: anti-Podocalyxin (R&D, 1:400) and anti-Coll IV (AbD Serotech, 1:200). Secondary antibodies for immunofluorescence were donkey antibodies to the appropriate species conjugated with Alexa Fluor 488, 555 or 647 (dilution 1:200 or 1:400).

**Plasmids.** Mouse Pix-α-FL fused to HA-tag was amplified with primers SG57-F and SG56-R (Supplementary Table 9) and was cloned in pcDNA3.1(+) vector (Invitrogen), whereas Pix-α-Δ17 was generated by PCR-mediated mutagenesis of Pix-α-FL (using primers SG55-F/-R and SG56-F/-R). All constructs were verified by sequencing.

**RNA extraction and RT-PCR.** Total RNA was isolated using the RNeasy Mini Kit (QIAGEN) according to the manufacturer's instructions. After treatment with DNase (Ambion), 2–3 µg of RNA was retro-transcribed with mix of d(T)<sub>18</sub> oligos and random hexamers or gene-specific primers (Supplementary Table 10) and Superscript III RT (Invitrogen). An aliquot (1/20th) of RT was then PCR-amplified. For qPCR, an aliquot of the RT reaction was analysed with QuantiTect SYBR Green PCR (QIAGEN) by using LyghtCycler 480 (Roche). Target transcript levels were normalized to those of reference gene. The expression of each gene was measured in at least three independent experiments. All primers are listed in Supplementary Tables 6 and 7. AS bands were quantified using densitometric analysis.

**Pull down of GTP-bound Cdc42.** Nova2-depleted and control mouse ECs cultured in 100-mm Petri dishes were analysed for Cdc42 activity by using the Cdc42 Activation Assay Kit (Abcam) according to the manufacturer's instructions. For experiments with Pix-α minigenes, cells were transfected with Lipofectamine 3000 (Invitrogen) and grown to reach confluence before the beginning of the pull down.

**Zebrafish strains and maintenance.** Zebrafish (*Danio rerio*) from wild-type AB and transgenic *Tg(fli1a:EGFP)y1* (ref. 41) strains were maintained and bred according to the national guidelines (Italian decree '4 march 2014, n.26'). All experimental procedures were approved by the FIRC Institute of Molecular Oncology Institutional Animal Care and Use Committee.

**In situ hybridization on zebrafish embryos and sections.** Zebrafish *nova2* cDNA was amplified using PCR (primers CG13F and CG13R in Supplementary Table 9) and cloned into pCRII-TOPO vector (Invitrogen). The antisense RNA probe was generated using T7 RNA Polymerase and digoxigenin-labelled UTPs (kit from Roche) and was purified with the RNeasy Mini Kit (QIAGEN) according to the

manufacturer's instructions. Whole embryos of different developmental stages were fixed overnight in 4% PFA, washed in PBS and pre-incubated for 2 h at 63 °C in hybridization buffer. Next, the *nova2* probe was added to the mix and incubated overnight at 63 °C. Embryos were then washed in SSC buffer and pre-incubated for 2 h in blocking medium at room temperature. A ratio of 1:2,000 anti-DIG antibody conjugated with alkaline phosphatase (Roche) was added and incubated overnight at 4 °C. After several PBS washes, embryos were incubated in NBT/BCIP staining buffer. Stained embryos were then equilibrated in glycerol 85% in PBS overnight at 4 °C and were observed with a stereomicroscope equipped with optic fibres. To prepare 50-µm transversal sections of 48-hpf embryos, previously stained by *in situ* hybridization, we cut them in PBS with a vibratome after inclusion in 5% low-melting agarose. Sections obtained were equilibrated and mounted in glycerol 85% in PBS on glass slides and observed under a Nikon Upright microscope. All images were acquired with high-resolution digital cameras (Nikon).

To detect the mRNA expression of *Rap1gap* and *Pix-α/Arhgef6* genes and GFP, we use 5-µm paraffin sections of the head of 48-hpf *Tg(fli1a:EGFP)y1* embryos fixed overnight with 4% PFA in PBS. To orientate embryos in the proper way before including in paraffin and cutting microtome sections, we have pre-included them in 1% low-melting agarose (in PBS) under a dissecting microscope with optic fibers, using plastic base moulds of 7 mm of diameter. Paraffin was removed with xylene and sections were rehydrated through graded EtOH washes, permeabilized with Proteinase-K and HCl 2N and were incubated overnight at 64 °C in hybridization mix with DIG-labelled LNA probes for *Rap1gap* (5'-TTCACCTCTT CACAGACAAGCT-3') and *Pix-α/Arhgef6* (5'-TAGACGTAGAGGTGTTGG ACT-3') (designed and produced by Exiqon). Sections were then treated overnight at 4 °C with an anti-DIG antibody (1:2,000 Roche) conjugated with AP and stained with NBT/BCIP. After several washes in PBS, embryo sections were incubated overnight at 4 °C with mouse anti-GFP antibody (Upstate, 1:200) and labelled using the *Vina Green Chromogen kit* (Biocare Medical).

**Zebrafish haematoxylin-eosin staining and immunofluorescence.** Agarose was used to embed 24- and 48-h zebrafish embryos before including in paraffin and cutting microtome 10-µm sections. Sections were stained with haematoxylin-eosin to assess the histological features. For immunofluorescence, paraffin was removed with xylene and the sections were rehydrated in graded alcohol. Antigen retrieval was carried out using preheated target retrieval solution (pH 6.0) for 45 min. Tissue sections were blocked with FBS serum in PBS for 90 min and incubated overnight with the following primary antibodies: GFP (1:100 Millipore), Phosphohistone H3 (PHH3, 1:100 Millipore), Caspase3 (1:100 Cell Signaling) and Podocalyxin (Podxl2 1:200, kindly provided by Heinz-Georg Belting). Alexa Fluor-conjugated antibodies were used for the immunodetection, and all sections were counterstained with 4,6-diamidino-2-phenylindole (DAPI) and visualized using a Confocal microscope (Leica SP2).

**Morpholino injections and RT-PCR of zebrafish embryo.** Zebrafish embryos at one- to two-cell stage were injected with 6.7 ng of an ATG-morpholino antisense oligonucleotide (Supplementary Table 8), designed to block translation of the zebrafish *nova2* gene (ENSDARG00000017673). To analyse the kinetics and the pattern of formation of the ISVs, we mounted in 1.2% low-melting agarose in E3 water *Tg(fli1a:EGFP)y1*-dechorionated embryos at 22 hpf, previously anaesthetized using 15 mg l<sup>-1</sup> of tricaine (Sigma). Image acquisition was performed overnight every 10 min with a ×40 water immersion objective on a Leica TCS SP2 confocal microscope. Confocal stacks from each time point were processed for maximum intensity projections and, subsequently, movies were generated with the Leica LCS software. To observe and evaluate the shape and function of the heart, we mounted under a stereomicroscope 48-hpf dechorionated embryos in 3% methyl-cellulose in E3 water, previously anaesthetized using 15 mg l<sup>-1</sup> of tricaine (Sigma). Using high-resolution digital camera (Nikon), we acquired 13-s movies from both control and *nova2* morphant embryos. Total RNA was extracted from 24-hpf pooled embryos with TRIzol reagent (Invitrogen), purified with the RNeasy Mini Kit (QIAGEN) and retro-transcribed with d(T)<sub>18</sub> oligo or gene-specific primer and Superscript III RT (Invitrogen) and then analysed in PCR for AS modification of *nova2* targets. To rescue morphological and vascular defects due to the knockdown of *nova2*, we amplified with primers CG30F/CG13R (Supplementary Table 9) by using RT generated from *Tg(fli1a:EGFP)y1* embryos, a morpholino-resistant zebrafish *nova2* cDNA, with six mismatches in the pairing region with the morpholino, which, however, do not alter the amino-acid sequence of the translated protein. We cloned this cDNA in pCRII-TOPO vector (Invitrogen) and we transcribed *in vitro* the capped mRNA using SP6 mMessage mMachine kit (Ambion). Co-injection in one- to two-cell stage embryos of 6.7 ng of MO-*nova2* and 160 pg of each *nova2* mRNAs was performed. The molecular and morphological changes of *nova2* morphants were scored at 28 hpf.

**Generation of new fish line for endothelial-specific rescue.** To drive Nova2 expression selectively in the zebrafish vascular endothelium, we cloned the morpholino-resistant zebrafish *nova2* cDNA into the pTolfliepCherryDest vector<sup>56</sup> in frame with mCherry at the N terminus under the endothelial *fli1a* enhancer/promoter flanked by Tol2 transposable elements (*pTolfliepCherryDest*). Fertilized eggs from *casper* × *Tg(fli1a:EGFP)y1* mutant/transgenic line were injected

with 2 nl of a mixture containing 25 ng  $\mu\text{l}^{-1}$  of the circular plasmid *pTolfl1:nova2-CherryDest* and 25 ng  $\mu\text{l}^{-1}$  of T2 transposase mRNA. Injected embryos were selected for simultaneous expression of GFP and mCherry in the vessels, raised to adulthood and crossed with *casper*  $\times$  *Tg(fli1a:EGFP)y1* fish. F1 embryos were observed under a fluorescent dissecting microscope from days 1 to 5 after fertilization to select carrier fish of the new mutant/double transgenic line *casper*  $\times$  *Tg(fli1a:EGFP)y1* + *Tg(fli1a:nova2-mCherry)*.

To assay the capability of *nova2* mRNA to rescue *nova2* morphant phenotype specifically in the vessel endothelium, we performed two experiments. Co-injection of 6.7 ng of MO-*nova2*, 50 pg of the rescuing DNA construct *pTolfl1:nova2-CherryDest* and 120 pg of Tol2 transposase mRNA was performed directly into the cytoplasm of one-cell stage *casper*  $\times$  *Tg(fli1a:EGFP)y1* embryos. The phenotype of the vessels of the resulting 'mosaic' embryos was scored at 28 hpf. Alternatively, injection of 6.7 ng of MO-*nova2* was performed into one-cell stage *casper*  $\times$  *Tg(fli1a:EGFP)y1* + *Tg(fli1a:nova2-mCherry)* embryos. The phenotype of all the vessels of the resulting embryos was scored at 28 hpf.

**Immunofluorescence staining of zebrafish embryos.** Zebrafish embryos from the *Tg(fli1a:EGFP)y1* strain at 48 hpf were dechorionated and fixed in 2% PFA in PBS, overnight at 4 °C. Embryos were then washed four times for 5 min in PBST (PBS + 0.1% Tween20). Permeabilization in PSBT + 0.5% Triton X-100 was performed for 30 min at room temperature. Embryos were then blocked in a solution of PBST + 0.5% Triton X-100, 10% normal goat serum and 1% BSA for 2 h at room temperature. Embryos were incubated with primary antibodies in blocking solution overnight at 4 °C. Successively, embryos were washed six times in PBST over 4 h at room temperature and then incubated with secondary antibodies in blocking solution, overnight at 4 °C. Embryos were washed finally six times in PBST over 4 h at room temperature and equilibrated in glycerol 85% in PBS. The following antibodies were used: mouse anti-GFP (1:2,000 Millipore); rabbit anti-podocalyxin (1:150 kindly provided by Heinz-Georg Belting); rabbit anti-mouse Alexa-488-conjugated IgG (1:400); and goat anti-rabbit Alexa 546-conjugated IgG (1:400). For the microscope analysis, we mounted on slides the trunk and tail regions dissected from five to six embryos of each samples. Images were taken with a Leica TCS SP2 confocal microscope, using oil-immersion objective  $\times 40$ .

**Generation of *nova2* zebrafish mutant by CRISPR/Cas9.** To identify the best target site and to design the single guide RNA (gRNA), we submitted to the ZiFiT targeter website (<http://zifit.partners.org/ZiFiT>) the sequence of the first exon of the zebrafish *nova2* gene. Oligonucleotides corresponding to the target region (see Supplementary Fig. 11A and Supplementary Table 11) were annealed and cloned into the pDR274 gRNA expression vector (Addgene, 42250) immediately upstream of the crRNA:tracrRNA backbone. The *nova2* genomic target sequence starts with two GG nucleotides at the 5' end for efficient transcription from the T7 promoter and ends with the protospacer-adjacent motif. The correct position of the target sequence into the pDR274 plasmid was verified through sequencing, using M13-Rev primer (Supplementary Table 11). The *nova2* gRNA was *in vitro* transcribed and purified from DraI-digested plasmid as template, using the Maxiscript T7 Kit (Life Technologies). Capped and polyadenylated *Cas9* mRNA was *in vitro* transcribed and purified from 1  $\mu\text{g}$  of PmeI-digested pMLM3613 *Cas9* expression vector (Addgene, 42251) as a template, using the mMessage mMachine T7 ULTRA kit (Life Technologies).

A volume of 2 nl of a solution containing  $\sim 13$  ng  $\mu\text{l}^{-1}$  of *nova2* gRNA and  $\sim 300$  ng  $\mu\text{l}^{-1}$  of *Cas9* mRNA was co-injected in one-cell stage zebrafish embryos. On the next day, only embryos with a normal morphological phenotype were allowed to grow. To evaluate the efficiency of *Cas9* nuclease activity, genomic DNA was extracted from 48-hpf single injected embryos and the *nova2*-targeted genomic locus was amplified from genomic DNA of each embryo (primers n2-locus-F and n2-locus-R in Supplementary Table 11). PCR products were then processed for the T7 Endonuclease I (T7EI) assay. PCR products were denatured at 95 °C and rapidly re-annealed using a PCR thermocycler. PCR products were then incubated for 20 min with T7EI enzyme at room temperature, and the digestion products were visualized on 2% agarose gels. We found that 95% of the injected embryos had mutations at the level of the *nova2* target site.

To analyse the kinds of mutations obtained at the level of the *nova2* locus, we sequenced PCR products, cloned into pCRII-TOPO plasmid using the TOPO TA cloning kit (Life Technologies), amplified from genomic DNA extracted from fin-fragments of 2-month fishes. Among these fishes, we isolated those carrying the mutation also in the germline and subsequently we selected from their progeny fishes with nonsense or missense mutations in the *nova2* locus. A male carrying a nonsense mutation was crossed with a female from the *Tg(kdr:EGFP)* line to generate a double *EGFP* transgenic-*nova2* mutant line expressing the *EGFP* reporter in vascular ECs and allowing to characterize the vascular phenotype of *nova2* mutants.

**o-dianisidine staining.** For histochemical staining of haemoglobin, 72 hpf live embryos were incubated with o-dianisidine staining solution (40% ethanol, 0.01 M sodium acetate, 0.65%  $\text{H}_2\text{O}_2$ , 0.6 mg  $\text{ml}^{-1}$  o-dianisidine (Sigma, D-9143) for 15 min. Embryos were then washed with PBS, post-fixed in 4% PFA in PBS overnight at 4 °C and stored in 85% glycerol for microscope analysis.

**RNAseq and splicing analysis.** RNAseq was conducted on two control and two *Nova2*-depleted ECs. Samples were sequenced on Illumina HiSeq2500 (average of  $\sim 93$  million, 100-nucleotide (nt) paired-end reads for each run). We employed *vast-tools*<sup>52</sup> to identify and quantify all major types of AS events, including single and multiple cassette exons and microexons, alternative 5' and 3' splice sites and alternatively retained introns, from each RNAseq sample. *vast-tools* map reads to comprehensive sets of exon-exon junctions (EEJs) and exon-intron junctions (EIJs) to derive alternative sequence inclusion levels (PSIs, 'Percent Spliced In', for exons; PIR, 'Percent Intron Retention', for introns)<sup>57</sup>. We then compared the two replicates of *Nova2* knockdown ECs versus control ECs. Differentially regulated AS events were defined as those showing an absolute  $\Delta\text{PSI} \geq 15$  between knockdown and control means and a  $\Delta\text{PSI} \geq 5$  between the ranges of the two groups. Only AS events with a minimum read coverage in all four samples were compared, which was defined as:

- For cassette exons (except for those quantified using the microexon pipeline, see Irimia *et al.*<sup>52</sup> for details): (i)  $\geq 10$  reads mapping to the sum of exclusion EEJs or (ii)  $\geq 10$  reads mapping to one of the two inclusion EEJs and  $\geq 5$  to the other inclusion EEJ.
- For microexons: (i)  $\geq 10$  reads mapping to the sum of exclusion EEJs or (ii)  $\geq 10$  reads mapping to the sum of inclusion EEJs.
- For intron retention: (i)  $\geq 10$  reads mapping to the sum of skipping EEJs or (ii)  $\geq 10$  reads mapping to one of the two inclusion EIJs and  $\geq 5$  to the other inclusion EIJ.
- For alternative 3' and 5' splice sites:  $\geq 10$  reads mapping to the sum of all EEJs involved in the specific event.

Additional filtering was used to remove intron retention events with a binomial *P* value score above 0.05 in any of the four samples<sup>57</sup>.

This resulted in 365 differentially regulated AS events (Supplementary Fig. 4 and Supplementary Table 1), which were subdivided according to the predicted impact of *Nova2* knockdown on the coding sequence (Supplementary Fig. 5A): (i) AS events predicted to generate protein isoforms both when *Nova2* is present or depleted (150, 41.1%); (ii) AS events predicted to trigger nonsense-mediated decay (NMD) or create a truncated protein when *Nova2* is present (135, 37.0%); (iii) AS events predicted to trigger NMD or to create a truncated protein when *Nova2* is absent (33, 9.0%); (iv) AS events in noncoding regions (40, 11.0%); and (v) AS events not able to be categorized into previous categories (7, 2%).

GO analysis was performed for each of the subdivided groups using ClueGO<sup>58</sup>. The background reference was based on multiexonic genes with the same minimum read coverage in the endothelium used above. Two categories had significant enrichment (*P* value < 0.05), those generating protein isoforms ((i) 49 terms enriched in 150 genes; Supplementary Fig. 5B) and those predicted to trigger NMD/disrupted proteins when *Nova2* is included ((ii) 15 terms enriched in 135 genes; Supplementary Fig. 5C). Detail of *P* values (as calculated by ClueGO) are found in Supplementary Table 2.

To compare AS events that show differential inclusion on *Nova2* knockdown in ECs to those regulated by *Nova* proteins in neural cells, we used the 325 cassette exons previously predicted to be *Nova* targets in the brain<sup>33</sup> (Supplementary Table 3). Nearly all (319/325) exons could be matched to *vast-tools* AS event IDs based on the exact splice site coordinates and official gene symbols. Of these, 195/319 (61%) had enough read coverage to confidently derive inclusion estimates (PSIs) in all four EC RNAseq samples. From these, 28/195 (14.4%) exons showed a  $\Delta\text{PSI} \geq 10$  on *Nova2* knockdown in ECs in the same direction as previously predicted for *Nova* proteins in the brain, compared with only 2/195 (1%) in the opposite direction (Supplementary Fig. 6). This overlap between *Nova*-regulated exons in endothelial and neural cells is highly significant ( $P = 1.93e^{-11}$ , hypergeometric test; background event set corresponded to 14,970 cassette exons with a minimal read coverage in the endothelium as described above and in genes with a  $\text{cRPKM} > 2$  in neurons<sup>19</sup>). Moreover, several methodological differences suggest that the actual overlapping of *Nova2* regulation between endothelial and neural cells may be even higher. First, predictions of Zhang *et al.*<sup>33</sup> include *Nova1* and *Nova2* targets, which may not be fully redundant. Second, exons described in Zhang *et al.* are predicted to be *Nova* protein targets based on *Nova* binding and presence of binding sites, among others. However, only half of the full set of *Nova* targets shows measurable differences in PSI in *Nova* knockout mice<sup>33</sup>. Finally, *Nova2* proteins may use different cofactors that may be differentially expressed between endothelial and neural cells.

## References

1. Chung, A. S. & Ferrara, N. Developmental and pathological angiogenesis. *Annu. Rev. Cell Dev. Biol.* **27**, 563–584 (2011).
2. Potente, M., Gerhardt, H. & Carmeliet, P. Basic and therapeutic aspects of angiogenesis. *Cell* **146**, 873–887 (2011).
3. Zacchigna, S., Lambrechts, D. & Carmeliet, P. Neurovascular signalling defects in neurodegeneration. *Nat. Rev. Neurosci.* **9**, 169–181 (2008).
4. Segura, I., De Smet, F., Hohensinner, P. J., Ruiz de Almodovar, C. & Carmeliet, P. The neurovascular link in health and disease: an update. *Trends Mol. Med.* **15**, 439–451 (2009).

5. Pan, Q., Shai, O., Lee, L. J., Frey, B. J. & Blencowe, B. J. Deep surveying of alternative splicing complexity in the human transcriptome by high-throughput sequencing. *Nat. Genet.* **40**, 1413–1415 (2008).
6. Wang, E. T. *et al.* Alternative isoform regulation in human tissue transcriptomes. *Nature* **456**, 470–476 (2008).
7. Chen, M. & Manley, J. L. Mechanisms of alternative splicing regulation: insights from molecular and genomics approaches. *Nat. Rev. Mol. Cell Biol.* **10**, 741–754 (2009).
8. Nilsen, T. W. & Graveley, B. R. Expansion of the eukaryotic proteome by alternative splicing. *Nature* **463**, 457–463 (2010).
9. Blencowe, B. J. Alternative splicing: new insights from global analyses. *Cell* **126**, 37–47 (2006).
10. Le, K. *et al.* Detecting tissue-specific regulation of alternative splicing as a qualitative change in microarray data. *Nucleic Acids Res.* **32**, e180 (2004).
11. Pan, Q. *et al.* Revealing global regulatory features of mammalian alternative splicing using a quantitative microarray platform. *Mol. Cell* **16**, 929–941 (2004).
12. Palumbo, A. *et al.* A chemically modified antibody mediates complete eradication of tumours by selective disruption of tumour blood vessels. *Br. J. Cancer* **104**, 1106–1115 (2011).
13. Neri, D. & Bicknell, R. Tumour vascular targeting. *Nat. Rev. Cancer* **5**, 436–446 (2005).
14. Bazigou, E. *et al.* Integrin- $\alpha$ 9 is required for fibronectin matrix assembly during lymphatic valve morphogenesis. *Dev. Cell* **17**, 175–186 (2009).
15. Bazigou, E. *et al.* Genes regulating lymphangiogenesis control venous valve formation and maintenance in mice. *J. Clin. Invest.* **121**, 2984–2992 (2011).
16. Ule, J. *et al.* Nova regulates brain-specific splicing to shape the synapse. *Nat. Genet.* **37**, 844–852 (2005).
17. Taddei, A. *et al.* Endothelial adherens junctions control tight junctions by ve-cadherin-mediated upregulation of claudin-5. *Nat. Cell Biol.* **10**, 923–934 (2008).
18. Yang, Y. Y., Yin, G. L. & Darnell, R. B. The neuronal rna-binding protein nova-2 is implicated as the autoantigen targeted in poma patients with dementia. *Proc. Natl Acad. Sci. USA* **95**, 13254–13259 (1998).
19. Zhang, Y. *et al.* An rna-sequencing transcriptome and splicing database of glia, neurons, and vascular cells of the cerebral cortex. *J. Neurosci.* **34**, 11929–11947 (2014).
20. Yan, Q. *et al.* Systematic discovery of regulated and conserved alternative exons in the mammalian brain reveals nmd modulating chromatin regulators. *Proc. Natl Acad. Sci. USA* **112**, 3445–3450 (2015).
21. Ule, J. *et al.* An rna map predicting nova-dependent splicing regulation. *Nature* **444**, 580–586 (2006).
22. Hellström, M. *et al.* Dll4 signalling through notch1 regulates formation of tip cells during angiogenesis. *Nature* **445**, 776–780 (2007).
23. Iruela-Arispe, M. L. & Davis, G. E. Cellular and molecular mechanisms of vascular lumen formation. *Dev. Cell* **16**, 222–231 (2009).
24. Solecki, D. J., Govek, E., Tomoda, T. & Hatten, M. E. Neuronal polarity in CNS development. *Genes Dev.* **20**, 2639–2647 (2006).
25. Lampugnani, M. G. *et al.* Ccm1 regulates vascular-lumen organization by inducing endothelial polarity. *J. Cell Sci.* **123**, 1073–1080 (2010).
26. Koh, W., Mahan, R. D. & Davis, G. E. Cdc42- and rac1-mediated endothelial lumen formation requires pak2, pak4 and par3, and pkc-dependent signaling. *J. Cell Sci.* **121**, 989–1001 (2008).
27. Yamanaka, T. *et al.* Par-6 regulates apkc activity in a novel way and mediates cell-cell contact-induced formation of the epithelial junctional complex. *Genes Cells* **6**, 721–731 (2001).
28. Jaffer, Z. M. & Chernoff, J. P21-activated kinases: three more join the pak. *Int. J. Biochem. Cell Biol.* **34**, 713–717 (2002).
29. Strlič, B. *et al.* The molecular basis of vascular lumen formation in the developing mouse aorta. *Dev. Cell* **17**, 505–515 (2009).
30. Bayless, K. J. & Davis, G. E. The cdc42 and rac1 gtpases are required for capillary lumen formation in three-dimensional extracellular matrices. *J. Cell Sci.* **115**, 1123–1136 (2002).
31. Oubaha, M. *et al.* Formation of a pkc $\zeta$ / $\beta$ -catenin complex in endothelial cells promotes angiopoietin-1-induced collective directional migration and angiogenic sprouting. *Blood* **120**, 3371–3381 (2012).
32. Irimia, M. *et al.* A highly conserved program of neuronal microexons is misregulated in autistic brains. *Cell* **159**, 1511–1523 (2014).
33. Zhang, C. *et al.* Integrative modeling defines the nova splicing-regulatory network and its combinatorial controls. *Science* **329**, 439–443 (2010).
34. Sakurai, A. *et al.* Magi-1 is required for rap1 activation upon cell-cell contact and for enhancement of vascular endothelial cadherin-mediated cell adhesion. *Mol. Biol. Cell* **17**, 966–976 (2006).
35. Tsygankova, O. M., Wang, H. & Meinkoth, J. L. Tumor cell migration and invasion are enhanced by depletion of rap1 gtpase-activating protein (rap1gap). *J. Biol. Chem.* **288**, 24636–24646 (2013).
36. Baird, D., Feng, Q. & Cerione, R. A. The cool-2/ $\alpha$ -pix protein mediates a cdc42-rac signaling cascade. *Curr. Biol.* **15**, 1–10 (2005).
37. Liu, Z., Adams, H. C. 3. & Whitehead, I. P. The rho-specific guanine nucleotide exchange factor dbpA regulates breast cancer cell migration. *J. Biol. Chem.* **284**, 15771–15780 (2009).
38. Miyamoto, Y., Yamauchi, J., Sanbe, A. & Tanoue, A. Dock6, a dock-c subfamily guanine nucleotide exchanger, has the dual specificity for rac1 and cdc42 and regulates neurite outgrowth. *Exp. Cell Res.* **313**, 791–804 (2007).
39. Montero-Balaguer, M. *et al.* Stable vascular connections and remodeling require full expression of ve-cadherin in zebrafish embryos. *PLoS ONE* **4**, e5772 (2009).
40. Jelen, N., Ule, J., Zivin, M. & Darnell, R. B. Evolution of nova-dependent splicing regulation in the brain. *PLoS Genet.* **3**, 1838–1847 (2007).
41. Lawson, N. D. & Weinstein, B. M. In vivo imaging of embryonic vascular development using transgenic zebrafish. *Dev. Biol.* **248**, 307–318 (2002).
42. Quaegebeur, A., Lange, C. & Carmeliet, P. The neurovascular link in health and disease: molecular mechanisms and therapeutic implications. *Neuron* **71**, 406–424 (2011).
43. Hwang, W. Y. *et al.* Efficient genome editing in zebrafish using a CRISPR-Cas system. *Nat. Biotechnol.* **31**, 227–229 (2013).
44. Jensen, K. B. *et al.* Nova-1 regulates neuron-specific alternative splicing and is essential for neuronal viability. *Neuron* **25**, 359–371 (2000).
45. Ruggiu, M. *et al.* Rescuing Z<sup>+</sup> agrin splicing in Nova null mice restores synapse formation and unmasks a physiologic defect in motor neuron firing. *Proc. Natl Acad. Sci. USA* **106**, 3513–3518 (2009).
46. Seshiah, P., Miller, B., Myat, M. M. & Andrew, D. J. Pasilla, the drosophila homologue of the human nova-1 and nova-2 proteins, is required for normal secretion in the salivary gland. *Dev. Biol.* **239**, 309–322 (2001).
47. Irimia, M. *et al.* Stepwise assembly of the nova-regulated alternative splicing network in the vertebrate brain. *Proc. Natl Acad. Sci. USA* **108**, 5319–5324 (2011).
48. Pirraglia, C., Walters, J. & Myat, M. M. Pak1 control of e-cadherin endocytosis regulates salivary gland lumen size and shape. *Development* **137**, 4177–4189 (2010).
49. Ramahi, J. S. & Solecki, D. J. The par polarity complex and cerebellar granule neuron migration. *Adv. Exp. Med. Biol.* **800**, 113–131 (2014).
50. Martin-Belmonte, F. *et al.* Pten-mediated apical segregation of phosphoinositides controls epithelial morphogenesis through cdc42. *Cell* **128**, 383–397 (2007).
51. Choi, S. Y. *et al.* Cdc42 deficiency causes ciliary abnormalities and cystic kidneys. *J. Am. Soc. Nephrol.* **24**, 1435–1450 (2013).
52. Jin, Y. *et al.* Deletion of cdc42 enhances adam17-mediated vascular endothelial growth factor receptor 2 shedding and impairs vascular endothelial cell survival and vasculogenesis. *Mol. Cell Biol.* **33**, 4181–4197 (2013).
53. Zlokovic, B. V. The blood-brain barrier in health and chronic neurodegenerative disorders. *Neuron* **57**, 178–201 (2008).
54. Tollervy, J. R. *et al.* Analysis of alternative splicing associated with aging and neurodegeneration in the human brain. *Genome Res.* **21**, 1572–1582 (2011).
55. Ule, J. *et al.* Clip identifies nova-regulated rna networks in the brain. *Science* **302**, 1212–1215 (2003).
56. Villefranc, J. A., Amigo, J. & Lawson, N. D. Gateway compatible vectors for analysis of gene function in the zebrafish. *Dev. Dyn.* **236**, 3077–3087 (2007).
57. Braunschweig, U. *et al.* Widespread intron retention in mammals functionally tunes transcriptomes. *Genome Res.* **24**, 1774–1786 (2014).
58. Bindea, G. *et al.* ClueGO: a Cytoscape plug-in to decipher functionally grouped gene ontology and pathway annotation networks. *Bioinformatics* **25**, 1091–1093 (2009).

## Acknowledgements

We thank Professor Natan Lawson for pTolfl1epCherryDest plasmid; Dr Heinz-Georg Belting and Professor Markus Affolter for antibody against zebrafish Podxl2; Dr Davide Gabellini for helpful discussion; Dr Maria Paola Paronetto for critical reading of the manuscript; the IFOM (FIRC Institute of Molecular Oncology) Zebrafish Facility; DNA Sequencing Facility Unit—Cogentech *c/o* IFOM-IEO Campus; Professor Giuseppe Viale (IEO) for providing normal human tissues; Progetto d'Interesse Invecchiamento (CNR-MIUR). Dax Torti of the Donnelly Sequencing Centre is gratefully acknowledged for sequencing samples. This work was supported by grants from the Associazione Italiana per la Ricerca sul Cancro (AIRC, project 11913), the Association for International Cancer Research (AICR-UK, project 11–0622), Fondazione Banca del Monte di Lombardia to C.G.3 and grants from the Associazione Italiana per la Ricerca sul Cancro (AIRC, project 14471), 'Special Program Molecular Clinical Oncology 5 × 1000'—AGIMM (AIRC-Gruppo Italiano Malattie Mieloproliferative), the European Research Council (project EU-ERC 268870), the European Community (ITN VESSEL 317250), CARIPLO Foundation (project 2012-0678) and Telethon (project GGP14149) to E.D. Work in P.P.D.F. laboratory was supported by grants from the Associazione Italiana per la Ricerca sul Cancro (AIRC IG 14404 and MCO 10.000), MIUR (the Italian Ministry of University and Scientific Research), the Italian Ministry of Health and the Monzino Foundation. D.N. was supported by grants from the Swedish Research Council and the Swedish Society of Medical Research. C.D.R.W. is supported by a 'La Caixa/Severo



Ochoa' pre-doctoral fellowship. B.J.B. is supported by operating grants from the Canadian Institutes for Health Research and holds the Banbury Chair in Medical Research at the University of Toronto. S.G. is awarded a Fondazione Adriano Buzzati Traverso postdoctoral fellowship.

### Author contributions

C.G.<sup>1,2</sup> and S.G. designed and performed *in vitro* experiments; G.D., V.Q., E.B. and F.P. performed *in vivo* experiments in zebrafish embryos; D.N. performed analysis in mouse retina; S.C. and G.B.<sup>6</sup> performed the IHC analysis and discussed the results with PPDF; S.B., A.D.M., G.B.<sup>3</sup>, D.P., E.F.<sup>8</sup>, C.T., F.O. and E.F.<sup>7</sup> performed the experiments and discussed the results; C.D.R.W., M.I. and B.J.B. performed bioinformatic analysis and discussed the results; C.G.<sup>3</sup> and E.D. conceived and designed the study and wrote the manuscript.

### Additional information

**Accession codes.** RNASeq reads are available in the NCBI Sequence Read Archive, under Bioproject code PRJNA293346.

**Supplementary Information** accompanies this paper at <http://www.nature.com/naturecommunications>

**Competing financial interests:** The authors declare no competing financial interests.

**Reprints and permission** information is available online at <http://npg.nature.com/reprintsandpermissions/>

**How to cite this article:** Giampietro, C. *et al.* The alternative splicing factor Nova2 regulates vascular development and lumen formation. *Nat. Commun.* 6:8479 doi: 10.1038/ncomms9479 (2015).



This work is licensed under a Creative Commons Attribution 4.0 International License. The images or other third party material in this article are included in the article's Creative Commons license, unless indicated otherwise in the credit line; if the material is not included under the Creative Commons license, users will need to obtain permission from the license holder to reproduce the material. To view a copy of this license, visit <http://creativecommons.org/licenses/by/4.0/>